J|A|C|S
ARTICLES
Published on Web 06/14/2003

Spectroscopic and Computational Study of a Non-Heme Iron $\{Fe-NO\}^7$ System: Exploring the Geometric and Electronic Structures of the Nitrosyl Adduct of Iron Superoxide Dismutase

Timothy A. Jackson,[†] Emine Yikilmaz,[‡] Anne-Frances Miller,[‡] and Thomas C. Brunold*,[†]

Contribution from the Department of Chemistry, University of Wisconsin—Madison, Madison, Wisconsin 53706, and Department of Chemistry, University of Kentucky, Lexington, Kentucky 40506

Received November 29, 2002; E-mail: Brunold@chem.wisc.edu

Abstract: Like many non-heme iron enzymes, reduced iron superoxide dismutase (Fe^{2+}SOD) reacts with nitric oxide (NO) to yield an $\{Fe-NO\}^7$ system. Electron paramagnetic resonance (EPR) data obtained for this Fe−NO adduct of FeSOD (NO−FeSOD) exhibit two rhombic $S = 3/2$ signals of comparable population; $E/D = 0.128$ (42%) and 0.154 (58%). While similar results were previously reported for NO−FeSOD [Niederhoffer, E. C.; Fee, J. A.; Papaefthymiou, V.; Münck, E. Magnetic Resonance Studies Involving Iron Superoxide Dismutase from *Escherichia coli*. *Isotope and Nuclear Chemistry Division Annual Report*; Los Alamos National Laboratory: Los Alamos, NM, 1987], detailed geometric and electronic structure descriptions of these $\{Fe-NO\}^7$ systems had not yet been developed. Therefore, in addition to EPR spectroscopy, we have used electronic absorption, magnetic circular dichroism (MCD), variable-temperature, variable-field MCD, and resonance Raman spectroscopies to determine ground-state spin Hamiltonian parameters, electronic transition energies, oscillator strengths, and transition polarizations for NO−FeSOD. These spectroscopic parameters have been used in conjunction with density functional theory (DFT) and semiempirical INDO/S-CI calculations to generate an experimentally calibrated active site model for NO−FeSOD. Our studies indicate that NO binds to the active site of Fe^{2+}SOD to form a six-coordinate $\{Fe-NO\}^7$ system with an Fe−N−O angle of ∼145°. DFT computations performed on this model of NO−FeSOD reveal that the NO ligand is formally reduced by the ferrous center to yield NO^- and an Fe^{3+} center that are strongly antiferromagnetically coupled. DFT calculations reveal that NO binding to Fe^{2+}SOD also lowers the pK of the coordinated water ligand by at least 3.3 pH units, suggesting that this process is associated with increased acidity and probable ionization of the axial solvent ligand. To explore the origin of the two $\{Fe-NO\}^7$ systems observed by EPR spectroscopy, additional calculations have been performed on slightly perturbed NO−FeSOD models. Significantly, semiempirical INDO/S-CI computations reveal that the rhombicity of NO−FeSOD is altered by changes in the Fe−N−O angle or rotation about the Fe−N(O) bond, suggesting that the two species observed by EPR spectroscopy merely differ slightly with respect to the orientation of the NO ligand. Indeed, our EPR data obtained on NO−FeSOD variants indicate that the relative population of the $S = 3/2$ signals can be altered by perturbations in the second sphere of the protein active site. These results provide compelling evidence that the second coordination sphere is able to modulate the geometric and electronic structures of NO−FeSOD.

1. Introduction

Iron superoxide dismutase (FeSOD)[1] is a non-heme iron enzyme whose function is to disproportionate the toxic superoxide radical anion ($O_2^{\bullet -}$) to generate molecular oxygen and hydrogen peroxide.[2,3] FeSOD is structurally homologous to MnSOD,[4−6] though the two enzymes are not related to Cu,ZnSOD or NiSOD.[2,7,8] X-ray crystal structures have revealed that FeSOD from *Escherichia coli* (*E. coli*) is a homodimer with each subunit containing an iron ion coordinated with trigonal-bipyramidal geometry by three His residues, an Asp^- residue, and a solvent molecule, the latter of which is involved in an

* To whom correspondence should be addressed.
[†] University of Wisconsin—Madison.
[‡] University of Kentucky.

(1) Abbreviations: ADF, Amsterdam density functional; CI, configuration interaction; CT, charge transfer; DFT, density functional theory; EDTA, ethylenediaminetetraacetic acid; EPR, electron paramagnetic resonance; HOMO, highest occupied molecular orbital; INDO/S, intermediate neglect of differential overlap/spectroscopic parametrization; LF, ligand field; LMCT, ligand-to-metal charge transfer; LUMO, lowest unoccupied molecular orbital; MCD, magnetic circular dichroism; MO, molecular orbital; NMR, nuclear magnetic resonance; $PA_{(g)}$, gas-phase proton affinity; PCA, protocatechuate; 3,4-PCD, protocatechuate 3,4-dioxygenase; PDB, protein data bank; PIPES, piperazine-*N*,*N*′-bis(2-ethanesulfonic acid); RR, resonance Raman; SOD, superoxide dismutase; TACN, triazocyclononane; VTVH, variable-temperature, variable-field; WT, wild type; ZFS, zero-field splitting.

(2) Miller, A. F.; Sorkin, D. L. *Comments Mol. Cell. Biophys.* **1997**, *9*, 1−48.

10.1021/ja029523s CCC: $25.00

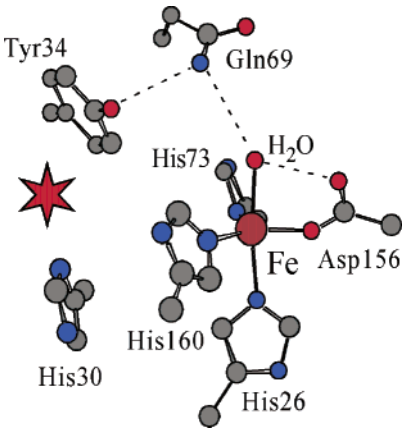

Figure 1. Active site model of Fe^{2+}SOD based on coordinates from the protein data bank file 1ISA. Dashed lines indicate hydrogen bonding interactions involving coordinated solvent, and the asterisk shows the position of the putative prebinding site. Hydrogen atoms have been omitted for clarity.

extensive hydrogen bond network (Figure 1).[4] This coordinated solvent molecule is proposed to be hydroxide in the oxidized form of the enzyme but acquires an additional proton upon metal ion reduction (eq 1).[9−11]

FeSOD reacts with superoxide in a two-step reaction mechanism according to eqs 2a,b.[12]

$$SOD(Fe^{3+}-OH^-) + e^- + H^+ \rightarrow SOD(Fe^{2+}-OH_2) \quad (1)$$

$$SOD(Fe^{3+}-OH^-) + O_2\bullet^- + H^+ \rightarrow SOD(Fe^{2+}-OH_2) + O_2 \quad (2a)$$

$$SOD(Fe^{2+}-OH_2) + O_2\bullet^- + H^+ \rightarrow SOD(Fe^{3+}-OH^-) + H_2O_2 \quad (2b)$$

As the rates of these reactions approach the diffusion limit,[12] no direct evidence exists for iron−superoxo or iron−peroxo intermediates that may be transiently formed during turnover. Therefore, much effort has gone into the characterization of FeSOD in the presence of substrate analogues.[12−15] While the ferric site of oxidized Fe^{3+}SOD is known to bind small anions such as azide and hydroxide to form six-coordinate ferric complexes,[4,9,15−17] reduced Fe^{2+}SOD is only known to bind anions in an outer-sphere fashion at a putative prebinding site (Figure 1);[8,12,18] thus, anions appear to coordinate to the ferric but not ferrous ion. However, it has been previously shown by EPR spectroscopy that Fe^{2+}SOD reacts with nitric oxide (NO) to form a complex that exhibits an $S = 3/2$ EPR spectrum.[19] Intriguingly, EPR data revealed the presence of two similar $S = 3/2$ species, both of which exhibit anomalously high rhombicities compared to other biological and synthetic Fe−NO complexes.[20−27] The main purpose of that study, however, was not to characterize the Fe−NO adduct(s) but rather to use NO as a means to probe the nature of the active site pK of Fe^{2+}SOD. Thus, while it has been known for 15 years that NO binds to Fe^{2+}SOD, little is known about the geometric and electronic structures of the complex(es) formed.

Nitric oxide is known to bind to a number of mononuclear non-heme iron enzymes,[19−25,28−31] in most cases forming complexes that can be classified as $\{Fe-NO\}^7$ systems according to the Enemark and Feltham notation, where the superscript denotes the number of 3d electrons on the Fe ion when the NO ligand is formally considered as NO^+.[32] In many of these studies, NO has been used as a probe of the ferrous state of the enzyme. While the ferric state of non-heme iron enzymes can be studied readily by EPR, optical absorption, and Mössbauer spectroscopies, the ferrous state of non-heme iron enzymes has long been considered spectroscopically inaccessible, as this state is EPR silent, and ligand field (LF) transitions associated with ferrous centers are typically so low in energy and weak in intensity that they often require the use of near-IR circular dichroism (CD) and magnetic CD (MCD) spectroscopies to be detected.[18] In contrast, $\{Fe-NO\}^7$ systems typically give rise to an $S = 3/2$ EPR signal and exhibit intense ligand-to-metal charge-transfer (LMCT) transitions that can be probed by UV−vis absorption spectroscopy.[20,22−25,30,31] Lipscomb and coworkers, among others, have used these spectroscopic signatures to probe interactions of non-heme iron enzymes with substrates, analogues, inhibitors, and solvent.[23,29,30,33,34] As Fe−NO adducts resemble putative $Fe-O_2$ species that may be transiently formed in the catalytic cycles of oxygen-activating enzymes, studies

(3) Valentine, J. S.; Wertz, D. L.; Lyons, T. J.; Liou, L.; Goto, J. J.; Gralla, E. B. *Curr. Opin. Chem. Biol.* **1998**, *2*, 253−262.
(4) Lah, M. S.; Dixon, M. M.; Pattridge, K. A.; Stallings, W. C.; Fee, J. A.; Ludwig, M. L. *Biochemistry* **1995**, *34*, 1646−1660.
(5) Edwards, R. A.; Baker, H. M.; Whittaker, M. M.; Whittaker, J. W.; Jameson, G. B.; Baker, E. N. *J. Biol. Inorg. Chem.* **1998**, *3*, 161−171.
(6) Ludwig, M. L.; Metzger, A. L.; Pattridge, K. A.; Stallings, W. C. *J. Mol. Biol.* **1991**, *219*, 335−358.
(7) Choudhury, S. B.; Lee, J. W.; Davidson, G.; Yim, Y. I.; Bose, K.; Sharma, M. L.; Kang, S. O.; Cabelli, D. E.; Maroney, M. J. *Biochemistry* **1999**, *38*, 3744−3752.
(8) Miller, A. F. In *Handbook of Metalloproteins*; Messerschmidt, A., Huber, R., Poulos, T., Wieghardt, K., Eds.; John Wiley & Sons: Chichester, U.K., 2001; pp 668−682.
(9) Tierney, D. L.; Fee, J. A.; Ludwig, M. L.; Penner-Hahn, J. E. *Biochemistry* **1995**, *34*, 1661−1668.
(10) Stallings, W. C.; Metzger, A. L.; Pattridge, K. A.; Fee, J. A.; Ludwig, M. L. *Free Radical Res. Commun.* **1991**, *12*−*13*, 259−268.
(11) Han, W.-G.; Lovell, T.; Noodleman, L. *Inorg. Chem.* **2002**, *41*, 205−218.
(12) Bull, C.; Fee, J. A. *J. Am. Chem. Soc.* **1985**, *107*, 3295−3304.
(13) Fee, J. A. *Mol. Microbiol.* **1991**, *5*, 2599−2610.
(14) Fee, J. A. *Biochem. J.* **1998**, *331*, 403−407.
(15) Xie, J.; Yikilmaz, E.; Miller, A. F.; Brunold, T. *J. Am. Chem. Soc.* **2002**, *124*, 3769−3774.
(16) Fee, J. A.; McClune, G. J.; Lees, A. C.; Zidovetzki, R.; Pecht, I. *Isr. J. Chem.* **1981**, *21*, 54−58.
(17) Jackson, T. A.; Xie, J.; Yikilmaz, E.; Miller, A. F.; Brunold, T. C. *J. Am. Chem. Soc.* **2002**, *124*, 10833−10845.
(18) Whittaker, J.; Solomon, E. I. *J. Am. Chem. Soc.* **1988**, *110*, 5329−5339.
(19) Niederhoffer, E. C.; Fee, J. A.; Papaefthymiou, V.; Münck, E. Magnetic Resonance Studies Involving Iron Superoxide Dismutase from *Escherichia coli*. *Isotope and Nuclear Chemistry Division Annual Report*; Los Alamos National Laboratory: Los Alamos, NM, 1987.
(20) Galpin, J. R.; Veldink, G. A.; Vliegenthart, J. F.; Goldingh, J. *Biochim. Biophys. Acta* **1978**, *536*.
(21) Salerno, J. C.; Siedown, J. N. *Biochim. Biophys. Acta* **1979**, *579*, 246−251.
(22) Arciero, D. M.; Lipscomb, J. D.; Huynh, B. H.; Kent, T. A.; Münck, E. *J. Biol. Chem.* **1983**, *258*, 14981−14991.
(23) Arciero, D. M.; Orville, A. M.; Lipscomb, J. D. *J. Biol. Chem.* **1985**, *260*, 14035−14044.
(24) Nelson, M. J. *J. Biol. Chem.* **1987**, *262*, 12137−12142.
(25) Chen, V. J.; Orville, A. M.; Harpel, M. R.; Frolik, C. A.; Surerus, K. K.; Münck, E.; Lipscomb, J. D. *J. Biol. Chem.* **1989**, *264*, 21677−21681.
(26) Brown, C. A.; Pavlosky, M. A.; Westre, T. E.; Zhang, Y.; Hedman, B.; Hodgson, K. O.; Solomon, E. I. *J. Am. Chem. Soc.* **1995**, *117*, 715−732.
(27) Chiou, Y.-M.; Que, L. *Inorg. Chem.* **1995**, *34*, 3270−3278.
(28) Twilfer, H.; Bernhardt, F. H.; Gersonde, K. *Eur. J. Biochem.* **1985**, *147*, 171−176.
(29) Arciero, D. M.; Lipscomb, J. D. *J. Biol. Chem.* **1986**, *261*, 2170−2178.
(30) Orville, A. M.; Lipscomb, J. D. *J. Biol. Chem.* **1993**, *268*, 8596−8607.
(31) Clay, M. D.; Cosper, C. A.; Jenney, F. J.; Adams, M. W. W.; Johnson, M. K. *Proc. Natl. Acad. Sci. U. S. A.* **2003**, *100*, 3796−3801.
(32) Enemark, J. H.; Feltham, R. D. *Coord. Chem. Rev.* **1974**, *13*, 339−406.
(33) Orville, A. M.; Chen, V. J.; Kriauciunas, A.; Harpel, M. R.; Fox, B. G.; Münck, E.; Lipscomb, J. D. *Biochemistry* **1992**, *31*, 4602−4612.
(34) Wasinger, E. C.; Davis, M. I.; Pau, M. Y. M.; Orville, A. M.; Zaleski, J. M.; Hedman, B.; Lipscomb, J. D.; Hodgson, K. O.; Solomon, E. I. *Inorg. Chem.* **2003**, *42*, 365−376.

performed on Fe−NO species in the presence of small molecules, such as substrate or inhibitors, may offer insight into possible ternary complexes formed during catalysis.[23] Furthermore, through the use of EPR and Mössbauer spectroscopies, the ground-state properties of the enzymatic {Fe−NO}^{7} systems can be explored. Such studies have revealed that, in the majority of cases, these systems are almost completely axial ($E/D \ll 0.10$).[23,27,31]

Despite the large number of non-heme iron enzymes that bind NO, the geometric and electronic structures of the resulting {Fe−NO}^{7} systems are typically inferred from a comparison with spectroscopic data of model complexes.[26,27] From detailed spectroscopic and computational studies of Fe(Me_3TACN)(NO)-(N_3)$_2$ and FeEDTA−NO, Solomon and co-workers concluded that the {Fe−NO}^{7} unit is best described as Fe^{3+} ($S = 5/2$) antiferromagnetically coupled to NO^- ($S = 1$), resulting in the $S = 3/2$ ground state observed by EPR spectroscopy.[26,35] This electronic structure description has been disputed by Rodriguez et al. who claimed that Mössbauer data of nitrosyl derivatives of deoxyhemerythrin as well as B3LYP density functional theory (DFT) computations performed on Fe(Me_3TACN)(NO)(N_3)$_2$ indicate that strong delocalization within the {Fe−NO}^{7} unit causes electrons to be almost equally shared.[36] However, a comprehensive Mössbauer study on complexes of the {Fe−NO}^{6,7,8} types, performed by Hauser et al.,[37] supports the description offered by Solomon and co-workers. Because absorption, EPR, and MCD data obtained from these and other model complexes are qualitatively similar to data obtained for enzymatic {Fe−NO}^{7} systems, it has been assumed that the biological Fe−NO adducts possess similar electronic properties as model complexes.[26,27]

To validate that assumption, we present here, to our knowledge, the most detailed spectroscopic/computational study of a non-heme iron {Fe−NO}^{7} system, the NO adduct of Fe^{2+}SOD (NO−FeSOD).[38] On the basis of EPR, electronic absorption, MCD, variable-temperature, variable-field (VTVH) MCD, and resonance Raman spectroscopic data, we conclude that the two complexes that were previously observed by EPR spectroscopy have nearly identical electronic structures. Through the use of semiempirical INDO/S-CI and DFT computations, we have generated spectroscopically calibrated geometric and electronic structure descriptions of the NO−FeSOD active site and have explored possible differences between the two complexes observed by EPR spectroscopy. While small anions do not appear to coordinate to the ferrous ion of Fe^{2+}SOD, our spectroscopic and computational data provide clear evidence that NO, an open-shell, redox-active diatomic species similar to substrate superoxide, does react with the ferrous ion to form a six-coordinate complex. In this process the NO ligand formally oxidizes the metal center, most likely causing coordinated water to release a proton, events that nicely mimic key steps in the reductive half reaction during turnover (eq 2b). Mechanistic implications of these data along with possible factors contributing to the different reactivities toward NO of Fe^{2+}SOD and oxygen-activating enzymes are discussed.

2. Experimental Section

(2.1) Sample Preparation. Wild-type FeSOD was purified from *E. coli* according to published procedures.[39,40] The specific activity of purified FeSOD was >6000 units/((mg of protein)/min). Fe-substituted manganese SOD (Fe(Mn)SOD) was isolated according to published procedures[41] in which MnSOD was treated with guanidine hydrochloride and EDTA to generate partially unfolded apo-MnSOD that was reconstituted with Fe. All proteins were isolated in the predominantly oxidized state. The FeSOD and Fe(Mn)SOD proteins used in this study were typically ~0.25−0.5 mM in 100 mM phosphate buffer (pH 7.0) or 100 mM PIPES buffer (pH 7.0), and all manipulations were carried out at 4 °C. More concentrated protein solutions were unstable in the presence of nitric oxide. To generate the NO adduct of FeSOD, oxidized FeSOD was placed in a sealed vial and oxygen was removed by purging the headspace with argon gas for 30 min. To prepare EPR and resonance Raman samples, oxidized FeSOD was then treated with excess dithionite, which immediately reduced the ferric center, as evidenced by the loss of visible absorption intensity. Since dithionite absorbs intensely in the UV, oxidized FeSOD was treated with only 1−2 equiv of dithionite to prepare optical absorption and MCD samples. The headspace of reduced FeSOD was then purged with alkali-scrubbed NO gas until the solution turned green (a process typically taking 5 min). This green solution was transferred via a gastight syringe to an argon purged cuvette, EPR tube, or Raman tube, depending on the nature of the experiment. To obtain MCD samples or EPR samples in the presence of a glassing agent, degassed glycerol was added to the green solution, and the sample was transferred to an argon-purged MCD cell or EPR tube. EPR samples for the NO adducts of Fe(Mn)SOD were prepared in a similar fashion; however, reduced Fe(Mn)SOD was first transferred to a chilled EPR tube and then treated with NO gas.

To determine if the FeSOD protein undergoes side reactions (e.g., nitrosation of Cys or Tyr residues) with higher order NO_x species that would alter the EPR spectrum of NO−FeSOD, EPR data were collected for various NO−FeSOD samples prepared by varying the incubation time between 5 and 30 min. As shown in Figure S1 (Supporting Information), the relative populations of the two $S = 3/2$ EPR signals is insensitive to incubation time with NO, suggesting that protein damage affecting the geometric and electronic structures of the NO−FeSOD species does not occur within the time scale of 5−30 min.

As it has been reported that generating aqueous solutions of NO that are completely free of nitrite is extremely difficult,[42,43] we performed a control experiment in order to evaluate the concentration of background nitrite present in our samples. The headspace of a control solution lacking protein and dithionite was purged with NO gas for 5 min. This solution was acidified to pH 2 by the addition of degassed HCl. The concentration of nitrite was estimated by monitoring the absorption at 372 nm ($\epsilon = 52\ M^{-1}\ cm^{-1}$).[44] Based on these experiments, the concentration of nitrite present in our samples of NO−FeSOD ranges from ~2−5 mM. This result suggests that reactive, higher order nitric oxide derivatives (e.g., nitrous anhydride, N_2O_3, that, in solution, exists in equilibrium with nitrite) may also be present in our samples.[45] The significance of these results is addressed in the Discussion.

(2.2) EPR Spectroscopy and Computer Simulation. EPR data were collected on a Bruker ESP 300E spectrometer equipped with an Oxford

(35) Zhang, Y.; Pavlosky, M. A.; Brown, C. A.; Westre, T. E.; Hedman, B.; Hodgson, K. O.; Solomon, E. I. *J. Am. Chem. Soc.* **1992**, *114*, 9189−9191.
(36) Rodriguez, J. H.; Xia, Y.-M.; Debrunner, P. G. *J. Am. Chem. Soc.* **1999**, *121*, 7846−7863.
(37) Hauser, C.; Glaser, T.; Eckhard, B.; Weyhermüller, T.; Wieghardt, K. *J. Am. Chem. Soc.* **2000**, *122*, 4352−4365.
(38) Note that the abbreviation NO−FeSOD does not imply that nitric oxide binds to the iron ion through the oxygen atom; rather this ligand coordinates the iron ion through the nitrogen atom.
(39) Slykhouse, T. O.; Fee, J. A. *J. Biol. Chem.* **1976**, *251*, 5472−5477.
(40) Sorkin, D. L.; Miller, A.-F. *Biochemistry* **1997**, *36*, 4916−4924.
(41) Vance, C. K.; Miller, A.-F. *Biochemistry* **1998**, *37*, 5518−5527.
(42) Wolak, M.; Stochel, G.; Hamza, M.; van Eldik, R. *Inorg. Chem.* **2000**, *39*, 2018−2019.
(43) We thank one of the reviewers for suggesting that nitrite may be present in our samples of NO−FeSOD.
(44) Goldstein, S.; Czapski, G. *J. Am. Chem. Soc.* **1995**, *117*, 12078−12084.
(45) Lewis, R. S.; Tannenbaum, S. R.; Deen, W. M. *J. Am. Chem. Soc.* **1995**, *117*, 3933−3939.

ESR 900 continuous flow cryostat and an Oxford ITC4 temperature system to monitor and regulate the temperature. The microwave frequency was monitored using a Varian EIP model 625A CW frequency counter. Additional data were recorded on a Bruker Elexsys E500 spectrometer equipped with an ER 4116DM cavity resonator, an Oxford Instruments ITC4 temperature controller, and an ESR900 helium flow cryostat. A bridge-mounted microwave counter (ER049X), and a field-frequency lock were employed. Spectra were recorded under essentially nonsaturating conditions using 9.3−9.4 GHz frequency and 100 kHz field modulation. Other parameters (field resolution, field sweep rate, conversion time, and time constant) were chosen such that the resolution was limited by the modulation amplitude and are given in the captions of Figure 2, Figure 8, and Figures S1 and S5. EPR data were corrected for background signals associated with the EPR cavity by the subtraction of a background spectrum.

EPR simulations were carried out by fitting experimental data, recorded at different temperatures, to the following spin Hamiltonian

$$\mathbf{H} = \beta \mathbf{g}\cdot\mathbf{H}\cdot\mathbf{S} + \mathbf{S}\cdot\mathbf{D}\cdot\mathbf{S} \quad (3)$$

assuming an $S = 3/2$ ground state and using the matrix diagonalization of the XSophe software suite.[46] For an $S = 3/2$ system, the turning points associated with the transitions within the $M_s = \pm 1/2$ and $\pm 3/2$ Kramers' doublets that define $g_{\mathrm{eff.}(x,y,z)}$ are related to real g values, $g_{\mathrm{real}(x,y,z)}$, and the rhombicity of the system, E/D, by[47]

$$g_{\mathrm{eff.}(x)} = g_{\mathrm{real}(x)}\{1 \pm [1 + 3(E/D)]/\sqrt{[1 + 3(E/D)^2]}\} \quad (4a)$$

$$g_{\mathrm{eff.}(y)} = g_{\mathrm{real}(y)}\{1 \pm [1 - 3(E/D)]/\sqrt{[1 + 3(E/D)^2]}\} \quad (4b)$$

$$g_{\mathrm{eff.}(z)} = g_{\mathrm{real}(z)}\{1 \pm (-2)/\sqrt{[1 + 3(E/D)^2]}\} \quad (4c)$$

Experimental values for $g_{\mathrm{real}(x,y,z)}$ and E/D can be determined from $g_{\mathrm{eff.}(x,y,z)}$ obtained by computer simulation using eqs 4a−c and assuming isolated Kramers' doublets with effective $S = 1/2$, or, in this case, directly from simulations obtained by matrix diagonalization of the spin Hamiltonian.[48,49] The axial zero-field splitting, D, may also be estimated if an EPR signal can be observed at a temperature T such that kT is comparable with D. Fits of the population of the excited-state doublet as a function of temperature to a Boltzmann distribution readily yield the energy of the excited state relative to the ground state.[50] For an $S = 3/2$ system, the ground-state and excited-state doublets are separated by Δ, where $\Delta^2 = 4D^2[1 + 3(E/D)^2]$.[51] E/D ratios were computed from $g_{\mathrm{eff.}(x,y,z)}$, and Δ was estimated from the temperature dependence. Simulations of the EPR spectrum at different temperatures were also performed to obtain an estimate for D. Superhyperfine interactions and strain terms in **g** and **D** were neglected, and simple line shapes were assumed to be Gaussian in frequency (g) space.

(2.3) Absorption and MCD Spectroscopies. Variable-temperature absorption and MCD spectra were recorded using a Jasco J-715 spectropolarimeter in conjunction with an Oxford Instruments SM-4000 8T magnetocryostat. Low-temperature absorption and MCD samples of NO−FeSOD were prepared in 55% (v/v) glycerol and 100 mM phosphate buffer (pH 7.0). VTVH MCD data were fit using software developed by Dr. Frank Neese[52] (MPI Mülheim, Germany).

(2.4) Resonance Raman Spectroscopy. Resonance Raman spectra were obtained upon excitation with an Ar^+ ion laser (Coherent I-305) in conjunction with a dye laser (Coherent 599-01, equipped with rhodamine 6G dye) with incident power in the 20−30 mW range using an ∼135° backscattering arrangement. Samples were kept in NMR tubes that were placed in an EPR dewar filled with liquid N_2 ($T = 77$ K). The scattered light was dispersed by a triple monochromator (Acton Research, equipped with 300, 1200, and 2400 g/mm gratings) and detected with a back-illuminated CCD camera (Princeton Instruments, 1340 × 100 pixels). A resonance Raman excitation profile was obtained by monitoring the intensity of the peak associated with NO−FeSOD relative to the ice peak at 228 cm^{-1} as a function of excitation wavelength.

(2.5) Computations. (A) Active Site Models. The active site models for NO−FeSOD, WT Fe^{2+}SOD, and WT Fe^{3+}SOD were generated using the PDB file of N_3−FeSOD (PDB file 1ISC), and the PDB files of reduced and oxidized FeSOD (PBD files 1ISA and 1ISB), respectively.[4] For all models, the Asp and His ligands were replaced by formate and imidazoles, respectively, and for the model of NO−FeSOD, azide was replaced with nitric oxide. The Cartesian coordinates for all active site models used in this study are included as Supporting Information.

(B) DFT Calculations. Full DFT energy minimizations and single-point calculations were performed using the Amsterdam Density Functional (ADF) 2000.02 software package[53−56] and were converged to the $M_s = 3/2$ state for NO−FeSOD, the $M_s = 2$ state for WT Fe^{2+}SOD, and the $M_s = 5/2$ state for WT Fe^{3+}SOD. These computations were carried out on a home-built cluster of eight Pentium III processors using an uncontracted triple-ζ Slater-type orbital (STO) basis set with a single set of polarization functions (ADF basis set IV), an integration constant of 4.0, and the Vosko, Wilk, Nusair[57] local density approximation with the nonlocal gradient corrections of Becke[58] and Perdew.[59] Core orbitals were frozen through 1s (O, N, C) and 2p (Fe). Models of NO−FeSOD with nonequilibrium geometries of the Fe−NO unit (e.g., changes in the Fe−N−O angle or rotation about the Fe−N(O) bond) were generated by systematically varying one structural parameter while all other coordinates were kept constant. DFT-predicted electronic transition energies for all systems studied were obtained using the method of Slater.[60]

Additional single-point DFT calculations were performed on the geometry-optimized NO−FeSOD structure using the ORCA 2.0 software package developed by Neese. A Gaussian polarized double-ζ valence orbital basis set and the Demon_J auxiliary basis set were used with the local density approximation of Perdew and Wang,[61] the gradient corrections of Becke[58] and Perdew,[59] and an integration grid of 3 (Lebedew 194 points). Results obtained from DFT calculations using the ADF 2000.02 and ORCA 2.0 software packages were virtually identical, and the latter program was utilized in conjunction with the gOpenMol program developed by Laaksonen[62,63] to generate boundary surface plots of molecular orbitals.

(C) Semiempirical Calculations. Semiempirical INDO/S-CI computations for active site models of NO−FeSOD were performed using the ORCA 2.0 software package. The ORCA program uses the INDO/S-CI model of Zerner and co-workers,[64,65] the valence-shell ionization potentials and Slater−Condon parameters listed by Bacon and Zerner,[66] the standard interaction factors $f_{p\sigma p\sigma} = 1.266$ and $f_{p\pi p\pi} = 0.585$, and

(46) Wang, D. M.; Hanson, G. R. *J. Magn. Reson. A* **1995**, *117*, 1−8.
(47) Pilbrow, J. R. *J. Magn. Res.* **1978**, *31*, 479−489.
(48) Bennett, B.; Holz, R. C. *Biochemistry* **1997**, *36*, 9837−9846.
(49) Bennett, B.; Holz, R. C. *J. Am. Chem. Soc.* **1997**, *119*, 1923−1933.
(50) Khangulov, S. V.; Pessiki, P. J.; Barynin, V. V.; Ash, G. C.; Dismukes, G. C. *Biochemistry* **1995**, *34*, 2015−2025.
(51) Pilbrow, J. R. *Transition Ion Electron Paramagnetic Resonance*; Oxford University Press: New York, 1990.
(52) Neese, F.; Solomon, E. I. *Inorg. Chem.* **1999**, *38*, 1847−1865.
(53) Baerends, E. J.; Ellis, D. E.; Ros, P. *Chem. Phys.* **1973**, *2*, 41.
(54) Versluis, L.; Ziegler, T. *J. Chem. Phys.* **1988**, *88*, 322−328.
(55) te Velde, G.; Baerends, E. J. *J. Comput. Phys.* **1992**, *99*, 84−98.
(56) Guerra, C. F.; Snijders, J. G.; te Velde, G.; Baerends, E. J. *Theor. Chem. Acc.* **1998**, *99*, 391−403.
(57) Vosko, S. H.; Wilk, L.; Nusair, M. *Can. J. Phys.* **1980**, *58*, 1200−1211.
(58) Becke, A. D. *J. Chem. Phys.* **1986**, *84*, 4524−4529.
(59) Perdew, J. P. *Phys. Rev. B* **1986**, *33*, 8822−8824.
(60) Slater, J. C. *The Calculation of Molecular Orbitals*; John Wiley & Sons: New York, 1979.
(61) Perdew, J. P.; Wang, Y. *Phys. Rev. B* **1992**, *45*, 13244−13249.
(62) Laaksonen, L. *J. Mol. Graphics* **1992**, *10*, 33.
(63) Bergman, D. L.; Laaksonen, L.; Laaksonen, A. *J. Mol. Graphics Modell.* **1997**, *15*, 301.
(64) Ridley, J.; Zerner, M. C. *Theor. Chim. Acta* **1973**, *32*, 111.
(65) Zerner, M. C.; Loew, G. H.; Kirchner, R. F.; Mueller-Westerhof, U. T. *J. Am. Chem. Soc.* **1980**, *102*, 589.
(66) Bacon, A. D.; Zerner, M. C. *Theor. Chim. Acta* **1979**, *53*, 21.

the following spin−orbit coupling constants: $\zeta_{3d}(Fe) = 400\ cm^{-1}$, $\zeta_{4p}(Fe) = 445\ cm^{-1}$, $\zeta_{2p}(N) = 76\ cm^{-1}$, and $\zeta_{2p}(O) = 150\ cm^{-1}$. Restricted open-shell Hartree−Fock calculations were tightly converged to the $S = 7/2$ ground state that served as the reference state for configuration interaction (CI) calculations. CI with single and double electron excitations (CISD) was then included between $S = 7/2$, $S = 5/2$, and $S = 3/2$ states. CISD active spaces for the octet, sextet, and quartet states included single electron excitations from the nine lowest energy doubly occupied MOs (DOMOs) to all singly occupied MOs (SOMOs) and the thirteen lowest energy virtual MOs. For the octet states, double electron excitations from the two highest energy DOMOs to the SOMOs and to the two lowest energy virtual MOs were included. For the sextet and quartet states, double electron excitations within the seven SOMOs were included. This INDO/S-CISD active space was also used for models of NO−FeSOD with nonequilibrium geometries of the Fe−NO unit and a model of NO−FeSOD with water as an axial ligand. For all INDO/S-CI calculations, completeness of the active space was confirmed by the insensitivity of calculated zero-field splitting (ZFS) parameters to the inclusion of additional one- and two-electron excitations.

(D) Δp*K* *Calculations.* Following a previously employed method[17] based on the pioneering work of Noodleman and co-workers,[11,67,68] the Δp*K* of the axially ligated water molecule of NO−FeSOD was calculated with respect to WT Fe^{2+}SOD using DFT. While in principle an absolute p*K* could be calculated for the solvent ligand of NO−FeSOD, this is computationally rather challenging as the calculation of absolute p*K* values requires predicting changes in solvation energies and zero-point energies between deprotonated and protonated states.[68] In calculating a Δp*K*, we are able to ignore these contributions under the assumption that changes in solvation energies and zero-point energies are similar between NO−FeSOD and WT Fe^{2+}SOD. This assumption appears reasonable as the corresponding active sites possess the same overall charge.

DFT energy minimizations were performed on models of NO−FeSOD with an axial hydroxide ligand (NO−$FeSOD^{OH}$) and an axial water ligand (NO−$FeSOD^{H2O}$), and the energies of these species at convergence were used to determine the gas-phase deprotonation energy of the axial water ligand for NO−FeSOD, ϵ_{deprot}[NO−FeSOD], according to eq 5a. The corresponding gas-phase deprotonation energy for WT Fe^{2+}SOD, $\epsilon_{deprot}[Fe^{2+}SOD]$, was calculated according to eq 5b.

$$\epsilon_{deprot}[NO{-}FeSOD] = \epsilon[NO{-}FeSOD^{OH}] + \epsilon[H^+] - \epsilon[NO{-}FeSOD^{H2O}] \quad (5a)$$

$$\epsilon_{deprot}[Fe^{2+}SOD] = \epsilon[Fe^{2+}SOD^{OH}] + \epsilon[H^+] - \epsilon[Fe^{2+}SOD^{H2O}] \quad (5b)$$

From these gas-phase deprotonation energies, $\Delta PA_{(g)}$, the difference in gas-phase proton affinity in kilocalories per mole between NO−FeSOD and WT Fe^{2+}SOD, was determined according to eq 6. Note that in calculating a $\Delta PA_{(g)}$, the $\epsilon[H^+]$ terms cancel. Finally, $\Delta PA_{(g)}$ was converted to a Δp*K* according to eq 7, where 1.37 is a standard conversion factor relating $PA_{(g)}$ in units of kilocalories per mole to p*K*.

$$\Delta PA_{(g)} = \epsilon_{deprot}[NO{-}FeSOD] - \epsilon_{deprot}[Fe^{2+}SOD] \quad (6)$$

$$\Delta pK = \{\Delta PA_{(g)}\}/1.37 \quad (7)$$

3. Results and Analysis

(3.1) Spectroscopy. (A) EPR Data. EPR data at 4 K of the Fe−NO adduct of FeSOD (NO−FeSOD) in the presence of 55% (v/v) glycerol are shown in Figure 2, top. EPR data of NO−FeSOD in the absence of glycerol (data not shown) are virtually identical to those presented in Figure 2, indicating that glycerol does not affect the ground-state properties of NO−FeSOD. Our EPR data of NO−FeSOD (Figure 2) are similar to those reported by Niederhoffer et al.,[19] also revealing the presence of two rhombic systems with similar *g* values. Qualitatively, these data are reminiscent of Fe−NO adducts of the {Fe−NO}^{7} type that give rise to $S = 3/2$ EPR signals.[20,22−26,30,31] Typically for these systems, $D > 0\ cm^{-1}$ and the spin Hamiltonian in eq 3 predicts two Kramers doublets ($M_s = \pm 1/2, \pm 3/2$, in the limit of $E/D = 0$), where the $\pm 1/2$ doublet lies at lower energy. At 4 K only this lowest doublet is populated and effective *g* values, $g_{eff.}$, of $g_{||} = g_{eff(z)} = 2.0$ and $g_\perp = g_{eff(x,y)} = 4.0$ are predicted in the axial limit ($E/D = 0$). A splitting of the $g_\perp$ signal, as observed for NO−FeSOD (Figure 2), is characteristic of a rhombic system. Most {Fe−NO}^{7} systems, however, exhibit EPR signals that are much more axial, $E/D \ll 0.1$,[23,27] reflecting the dominance of the ligand-field component associated with the NO ligand with respect to the electronic structure of the ferric center.[32]

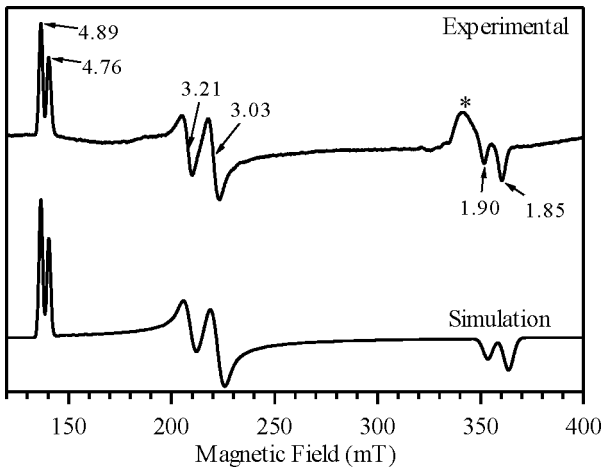

Figure 2. Top: EPR spectrum of NO−FeSOD in the presence of glycerol collected at 4 K, 9.3572 GHz microwave frequency, 1.27 mW microwave power, 1×10^5 receiver gain, 10.4 G modulation amplitude, 100 kHz modulation frequency, 5.12 ms time constant, and 2048 point resolution. Effective *g* values for EPR features associated with the {Fe−NO}^{7} systems are indicated. The asterisk marks EPR features associated with NO in frozen solution. Bottom: Simulated spectrum of two $S = 3/2$ species with $|D| \geq 6\ cm^{-1}$ and $E/D = 0.128$ (42%) and 0.154 (58%).

The EPR spectrum of NO−FeSOD recorded at 4 K was simulated (cf. Figure 2, top and bottom) assuming the presence of two $S = 3/2$ species of comparable populations (42 and 58%) and similar rhombicities ($E/D = 0.128$ and 0.154, respectively). The parameters used in the simulation of the major species were $g_{real} = 1.988, 2.000, 2.000$; $D = 6\ cm^{-1}$; and $E/D = 0.154$. These parameters correspond to g_{eff} values of 4.828, 3.022, and 1.865 (eq 4). The parameters used in the simulation of the minor species were $g_{real} = 1.998, 2.000, 2.010$; $D = 12\ cm^{-1}$; $E/D = 0.128$, yielding g_{eff} values of 4.705, 3.200, and 1.915 (eq 4). All of the observable g_{eff} values at 4 K are <5.4, indicating an $M_s = \pm 1/2$ ground state and thus a positive *D*. Note that the asymmetric peak at $g \sim 1.9$ is typical of free NO in frozen solution and therefore was not accounted for in the simulation.[69]

(67) Li, J.; Fisher, C. L.; Chen, J. L.; Bashford, D.; Noodleman, L. *Inorg. Chem.* **1996**, *35*, 4694−4702.
(68) Konecny, R.; Li, J.; Fisher, C. L.; Dillet, V.; Bashford, D.; Noodleman, L. *Inorg. Chem.* **1999**, *38*, 940−950.
(69) Wanat, A.; Schneppensieper, T.; Stochel, G.; van Eldik, R.; Bill, E.; Wieghardt, K. *Inorg. Chem.* **2002**, *41*, 4−10.

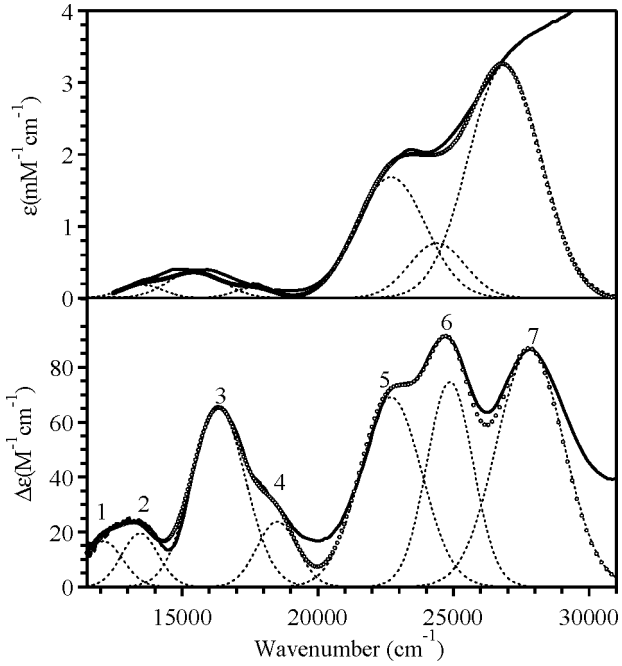

Figure 3. Room-temperature electronic absorption (top) and 7 T, 4.5 K MCD (bottom) spectra of NO−FeSOD. Individual Gaussian curves (dashed lines) and Gaussian fits (dotted lines) of the absorption and MCD data are displayed on their respective spectra.

The temperature dependence of the EPR signals associated with the $M_s = \pm 1/2$ doublet deviates significantly from Curie law behavior (Figure S2), indicating the population of the $M_s = \pm 3/2$ doublet at higher temperatures. From these data $D \sim 7$ cm^{-1} may be estimated. At higher temperatues (e.g., ~30 K) an additional resonance at $g_{eff} = 5.87$ (~200 mT) with a shoulder to low field was also observed, the presence of which indicates population of the $M_s = \pm 3/2$ doublets for the $E/D = 0.154$ and 0.128 species, respectively. The EPR spectrum of NO−FeSOD at 28 K (Figure S2) was simulated in order to further investigate the magnitude of D. Using the same simulation parameters as those for Figure 2, an estimate of $D = 6 \pm 1$ cm^{-1} was obtained for the dominant species (i.e. that exhibiting $E/D = 0.154$). This is significantly smaller than has been previously reported for other {Fe−NO}^{7} systems.[21,22,33,36] To our knowledge only two other examples of an {Fe−NO}^{7} system with $|D| < 10$ cm^{-1} exist: (i) the ternary adduct formed when reduced protocatechuate 3,4-dioxygenase (3,4-PCD) is treated with NO as well as substrate protocatechuate (PCA) or derivates of PCA ($D \sim 3-5$ cm^{-1})[30] and (ii) one of the $S = 3/2$ species formed by the addition of NO to superoxide reductase ($D \sim 5$ cm^{-1}).[31] The best estimate of D for the minor ($E/D = 0.128$) species was 12 cm^{-1}; however, the error in this estimation is large. Overall, our EPR data show that NO interacts with Fe^{2+}SOD to form two slightly different $S = 3/2$ species, both unusually rhombic for {Fe−NO}^{7} systems.

(B) Absorption, MCD, and VTVH MCD Data. Room-temperature electronic absorption data of NO−FeSOD are presented in Figure 3, top. The absorption spectrum exhibits the three-band pattern characteristic of six-coordinate Fe−NO adducts of the {Fe−NO}^{7} type of both inorganic complexes[26,27,37] and non-heme iron enzymes,[25,30,34,70] consisting of a weak, low-energy transition (~600 nm/(16 700 cm^{-1})) and two more intense, higher energy transitions (~450 nm/(22 200 cm^{-1}) and ~350 nm/(28 600 cm^{-1})). This result illustrates that NO binding to the ferrous active site of FeSOD does not result in ligand displacement, as a five-coordinate species would be expected to exhibit a very weak absorption feature at ~800 nm (12 500 cm^{-1}), a slightly more intense band at ~500 nm (20 000 cm^{-1}), and a very intense feature at ~350 nm (28 600 cm^{-1}).[71] Low-temperature absorption data of NO−FeSOD in the presence of glycerol (not shown) are virtually identical to the 300 K data in Figure 3, indicating that no major changes occur to the active site as the temperature is decreased.

The three characteristic absorption features of six-coordinate {Fe−NO}^{7} systems (cf. Figure 3, top) are typically attributed to electric dipole and spin-allowed NO^- $\pi^* \rightarrow Fe^{3+}$ LMCT transitions, as these transitions are expected to be intense in absorption.[26,30] For a ferric center with a d^5 electron configuration, all d→d (ligand field, LF) transitions are formally spin-forbidden and are thus not expected to carry significant absorption intensity. However, as the {Fe−NO}^{7} unit is best described as Fe^{3+} ($S = 5/2$) antiferromagnetically coupled to NO^- ($S = 1$) to give an $S = 3/2$ ground state,[26,37] exchange interactions between the ferric ion and the nitrosyl ligand could relax the spin selection rule, allowing d → d transitions to carry relatively large absorption intensities (vide infra).[72]

Low-temperature MCD data collected for NO−FeSOD are presented in Figure 3, bottom. While the absorption data permit identification of only three features, the MCD data reveal that at least seven electronic transitions occur in this spectral region. The lowest energy absorption band resolves into at least three MCD features; a very weak band at 13 000 cm^{-1} and an intense band at 16 500 cm^{-1} with a shoulder on its high-energy side. The two more intense absorption bands also resolve into three MCD features: a prominent shoulder at 22 000 cm^{-1} and two intense bands at 24 500 and 28 000 cm^{-1}. All of these MCD features are temperature dependent (Figure S3) and therefore may be assigned as MCD *C*-terms associated with a paramagnetic center.[52,73] Because there are no discernible MCD features in the near-IR spectral region below 12 000 cm^{-1} (data not shown), we conclude that our NO−FeSOD MCD data do not contain contributions from WT Fe^{2+}SOD, as the latter would give rise to a prominent positive feature at ~10 500 cm^{-1} ($\Delta\epsilon \sim 3.5$ M^{-1} cm^{-1}).[18] Likewise, the lack of an intense MCD feature at 26 000 cm^{-1} ($\Delta\epsilon \sim 35$ M^{-1} cm^{-1}) indicates that the amount of WT Fe^{3+}SOD in our samples is negligible.[17] Thus, we conclude that all evident transitions in the absorption and MCD spectra shown in Figure 3 are associated with NO−FeSOD.

To determine experimental transition energies and oscillator strengths, the room-temperature absorption and low-temperature MCD data were iteratively fit with a minimum number of Gaussian curves (Figure 3).[74] As the temperature is decreased, electronic transitions are expected to shift to slightly higher

(70) Haskin, C. J.; Ravi, N.; Lynch, J. B.; Münck, E.; Que, L. *Biochemistry* **1995**, *34*, 11090−11098.

(71) Ray, M.; Golombek, A. P.; Hendrich, M. P.; Yap, G. P. A.; Liable-Sands, L. M.; Rheingold, A. L.; Borovik, A. S. *Inorg. Chem.* **1999**, *38*, 3110−3115.

(72) Wheeler, D. E.; McCusker, J. K. *Inorg. Chem.* **1998**, *37*, 2296−2307.

(73) Piepho, S. B.; Schatz, P. N. *Group Theory in Spectroscopy with Applications to Magnetic Circular Dichroism*; John Wiley & Sons: New York, 1983.

(74) Low-temperature absorption data collected for NO−FeSOD were not suitable for quantitative analysis as these data were complicated by glass strain and were not as intense as the corresponding room-temperature data as the addition of glycerol reduced the concentration of NO−FeSOD.

Table 1. Absorption and MCD Transition Energies (cm^{-1}), Oscillator Strengths (f_{exp}), and Bandwidths (cm^{-1}) Based on a Gaussian Analysis of the Room-Temperature Absorption and Low-Temperature MCD Data of NO−FeSOD

band	energy	$f_{exp}{}^{a} \times 10^3$	fwhm[b]
1	abs: 12 100	0.17	1832
	MCD: 12 100		1665
2	abs: 13 500	1.55	1832
	MCD: 13 500		1581
3	abs: 15 500	4.10	2331
	MCD: 16 350		2331
4	abs: 17 750	1.29	1832
	MCD: 18 500		1748
5	abs: 22 700	23.20	2997
	MCD: 22 700		2664
6	abs: 24 400	8.49	2414
	MCD: 24 880		1998
7	abs: 26 900	47.20	3164
	MCD: 27 840		2914

[a] $f_{exp} = 4.32 \times 10^{-9} \int \epsilon(\nu))\, d\nu$, where $\epsilon(\nu)$ is the Gaussian line shape function of the appropriate band. [b] Full-width at half-maximum.

energy and to narrow in line width. Thus, the fitting procedure allowed for a slight blue-shifting and narrowing of the Gaussian curves used to reproduce the MCD data relative to those modeling the absorption data. This Gaussian analysis reveals the presence of seven transitions (Table 1), as expected on the basis of the qualitative analysis presented above. Based on their high absorption intensities and relatively large bandwidths, transitions 3, 5, and 7 (see Figure 3 for numbering scheme) are assigned as CT transitions. Conversely, transitions 1, 2, 4, and 6, which are relatively weak in the absorption spectrum but prominent in the MCD spectrum (cf. Figures 3, top and bottom), are assigned as d→d transitions. These transitions are able to acquire MCD intensity through spin−orbit coupling of the corresponding excited states with nearby CT excited states. In light of the fact that the spin−orbit coupling matrix elements are scaled by the energy difference between the interacting excited states, it is not surprising that transition 6, even though it does not markedly contribute to the absorption spectrum, is relatively intense in the MCD spectrum. Compared to the LF transitions observed in MCD data of WT Fe^{3+}SOD, which also gain intensity by excited-state spin−orbit coupling to nearby LMCT excited states, the LF transitions of NO−FeSOD carry considerably more MCD intensity (cf. $\Delta\epsilon \sim 5\ M^{-1}\ cm^{-1}$ for WT Fe^{3+}SOD versus $\Delta\epsilon \sim 20-70\ M^{-1}\ cm^{-1}$ for NO−FeSOD).[17,75] Additionally, our combined Gaussian analysis reveals that the visible region of the absorption spectrum of NO−FeSOD contains several LF transitions with absorption intensities that are greater than expected for a spin-uncoupled ferric center (Table 1).[76] Thus, while the large MCD and absorption intensities of the LF transitions associated with NO−FeSOD may be partially explained by spin−orbit coupling with intense LMCT transitions, exchange interactions between NO^- and Fe^{3+} may produce additional contributions to their high intensities.

Our spectral assignments for NO−FeSOD are consistent with previous studies carried out on synthetic $\{Fe-NO\}^7$ systems, which revealed that three intense NO^- $\pi^* \rightarrow Fe^{3+}$ CT transitions as well as several d→d transitions are expected in the visible spectral region.[26] However, while Brown et al. observed three NO^- $\pi^* \rightarrow Fe^{3+}$ CT transitions at similar energies (16 450, 18 440, and 21 000 cm^{-1}),[26] our analysis of absorption and low-temperature MCD data of NO−FeSOD reveals that one LMCT transition is significantly lower in energy than the two remaining LMCT transitions (Table 1). This difference reflects the unique electronic structure of NO−FeSOD compared to other $\{Fe-NO\}^7$ systems, the origin of which will be discussed in Computations below.

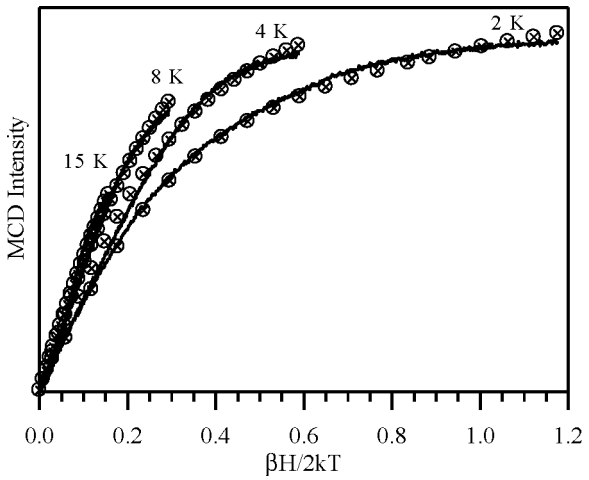

Figure 4. Experimental VTVH MCD data collected at 22 624 cm^{-1} (442 nm) for NO−FeSOD (solid lines) and theoretical fit (⊗).

Variable-temperature, variable-field MCD data collected at 22 624 cm^{-1} (Figure 4), as well as 27 777 and 16 339 cm^{-1} (Figure S4) are virtually identical, each data set showing similar nesting behavior. MCD magnetization saturation behavior is a sensitive function of ground-state spin Hamiltonian parameters as well as transition polarizations;[52,77] therefore, the high degree of similarity between VTVH MCD data collected at a variety of wavelengths indicates that these MCD *C*-terms i) are associated with species possessing very similar *g*-values and ZFS parameters and ii) originate from transitions that are similarly polarized. As the analysis of EPR data collected for NO−FeSOD has already provided ground-state spin Hamiltonian parameters, we have fit the VTVH MCD data by allowing the transition moment products (i.e., M_{xy}, M_{xz}, M_{yz}, where the coordinate system refers to the principal axis of the **D**-tensor) to be adjustable parameters. These transition moment products can then be related to the polarization of the electronic transition, giving rise to the observed saturation behavior.[52] The VTVH MCD data for NO−FeSOD collected at 22 624 cm^{-1} (442 nm) have been fit for $E/D = 0.154$ (Figure 4) and $E/D = 0.128$ (Figure S4). The fit presented in Figure 4 was obtained with <1% *x*-polarization, 19% *y*-polarization, and 81% *z*-polarization; however, further analysis revealed that the relative percentages of *y*- and *z*-polarizations are highly correlated, though the inclusion of any minor component of *x*-polarization led to significantly poorer fits. Similar polarizations were also used to successfully fit the identical VTVH MCD data assuming $E/D = 0.128$ (Figure S4); thus minor changes in the rhombicity alone do not deleteriously affect the goodness of fit. Fits were also performed where the magnitude of the axial ZFS parameter, *D*, was a variable. These data corroborate the *D* values determined

(75) Xie, J.; Brunold, T. Unpublished results.
(76) Solomon, E. I.; Brunold, T. C.; Davis, M. I.; Kemsley, J. N.; Lee, S. K.; Lehnert, N.; Neese, F.; Skulan, A. J.; Yang, Y. S.; Zhou, J. *Chem. Rev.* **2000**, *100*, 235−349.
(77) Oganesyan, V. S.; George, S. J.; Cheesman, M. R.; Thomson, A. J. *J. Chem. Phys.* **1999**, *110*, 762−777.

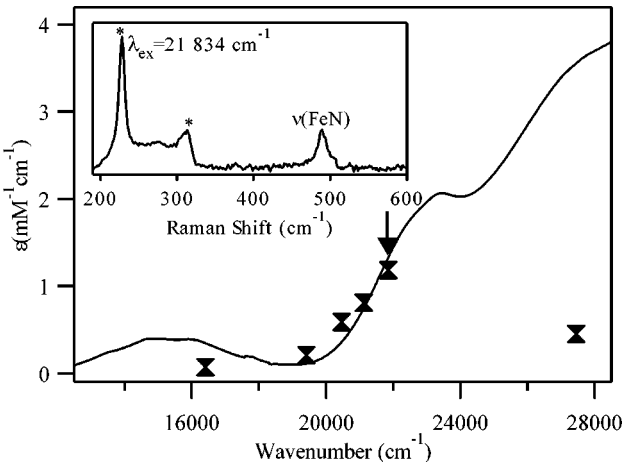

Figure 5. Superposition of electronic absorption spectrum (solid line) and resonance Raman excitation profile of the ν(FeN) vibration (symbol) for NO−FeSOD. The arrow indicates the excitation energy at which the resonance Raman spectrum, shown in the inset, was collected (21 834 cm^{-1} (458 nm)). Asterisks mark vibrations associated with the ice lattice.

by EPR spectroscopy, as the VTVH MCD data can be successfully fit with $D \sim 2-15$ cm^{-1}. Because VTVH MCD data collected at 16 339, 22 624, and 27 777 cm^{-1} are virtually identical, it can be concluded that the dominant features present in the MCD spectrum of NO−FeSOD all arise from transitions that are polarized perpendicular to the *x*-axis of the **D**-tensor. Overall, our MCD spectra and VTVH MCD data reveal that the two species contributing to the EPR spectrum of NO−FeSOD (Figure 2) must be very similar in nature.

(C) Resonance Raman Data. Resonance Raman (RR) data for NO−FeSOD obtained at 77 K with 21 834 cm^{-1} (458 nm) excitation are shown in Figure 5, inset. A prominent feature is observed[78] at 489 cm^{-1} that can be readily assigned to a vibration of the Fe−NO moiety by comparison to RR data reported for other {Fe−NO}^{7} systems[26,31,79] and by the absence of a corresponding feature in the RR spectra of WT Fe^{3+}SOD. Overall, three vibrations potentially giving rise to three RR peaks are expected to be associated with the Fe−NO unit: an N−O stretch, ν(NO), an Fe−N stretch, ν(FeN), and an Fe−N−O bend, δ(FeNO). The two vibrations involving the metal ion are expected to be at lower energy (∼390−600 cm^{-1}) than the intraligand vibration (∼1400−1900 cm^{-1}).[26,79,80] Of the two lower energy modes, typically ν(FeN) gives rise to a more intense RR peak than δ(FeNO).[31,79] Despite the fact that these three RR features associated with the {Fe−NO}^{7} unit are predicted, experimental observation of all three peaks is not always possible.[31,81] When both of the low-energy peaks are observed, one is typically very intense while the other is usually observed as a weak shoulder.[26,79] In principle, isotopic labeling can be used to assign these peaks to their respective vibrations, though such an analysis does not always yield unambiguous band assignments. While the position of δ(FeNO) is typically more sensitive to ^{15}N labeling than ν(FeN) (shifts of 6−15 cm^{-1} versus 1−6 cm^{-1}, respectively),[80] a normal coordinate analysis of the Fe−NO moiety with an angle of 155° predicted similar isotope shifts for the two modes (a shift of 9 cm^{-1} for δ(FeNO) and a shift of 6 cm^{-1} for ν(FeN)).[26] Additionally, hydrogen bonding has been shown to affect the isotopic sensitivity of the δ(FeNO) mode, appreciably reducing the ^{15}N isotope shift.[79] Therefore, we did not attempt to assign the RR spectrum of NO−FeSOD using ^{15}N isotopic labeling. However, based on the fact that ν(FeN) typically gives rise to more intense RR enhancement than δ(FeNO)[31,79] and supported by computational data provided below, we assign the peak at 489 cm^{-1} in the RR spectrum of NO−FeSOD (Figure 5, inset) to ν(FeN).

Figure 5 shows the RR excitation profile for ν(FeN). While the most significant RR enhancement of ν(FeN) occurs around 22 200 cm^{-1} (450 nm), there is still appreciable Raman enhancement in the higher energy region (∼27 000 cm^{-1}). These data reveal that bands 5 and 7 (see Figure 5 and Table 1) are associated with major perturbations of the Fe−NO moiety, supporting the assignment of these features as NO$^-$ → Fe^{3+} CT transitions. The differences in RR enhancement of ν(FeN) upon excitation in resonance with these two absorption bands may relate to differences in the nature of the donor and acceptor MOs involved in the corresponding transitions (vide infra). While it appears that band 3 shows little enhancement of ν(FeN), this band carries the weakest absorption intensity of all LMCT transitions, and the excitation wavelength (16 450 cm^{-1} (608 nm)) is slightly off resonance; thus, RR enhancement is expected to be weak in this region.

(D) Implications of Spectroscopic Data. Intriguingly, while the EPR data of NO−FeSOD indicate two $S = 3/2$ species of very similar populations, all other spectroscopic data are consistent with the presence of only one Fe−NO adduct. This observation suggests that the two $S = 3/2$ species observed by EPR spectroscopy possess similar geometric and electronic structures. By comparison with absorption data reported for other {Fe−NO}^{7} systems, it appears that NO binds to the active site of Fe^{2+}SOD to form a six-coordinate adduct.[25−27,30,37,70] However, NO−FeSOD differs from typical {Fe−NO}^{7} systems in its unusually high rhombicity.[21,22,30,31,33,36] Additionally, the splitting pattern of the NO$^-$ π^* → Fe^{3+} LMCT excited states appears to be altered relative to that of synthetic {Fe−NO}^{7} systems.[26] To further characterize NO−FeSOD and explore geometric and electronic differences between the two species observed by EPR spectroscopy, we have performed semiempirical INDO/S-CI and DFT computations on several hypothetical active site models.

(3.2) Computations. (A) Appropriate Model. As NO−FeSOD has not yet been crystallographically characterized, a hypothetical active site model was generated through the use of DFT energy minimization. The crystal structure of azide-bound Fe^{3+}SOD (PDB file 1ISC)[4] was used as a starting point, the active site was truncated as described in the Experimental Section, and azide was replaced with NO. While EPR data indicate an $S = 3/2$ ground state for this system, DFT computations do not permit the calculation of an $S = 3/2$ state for the {Fe−NO}^{7} unit (as the wave function for this state can only be expressed in terms of a linear combination of several Slater determinants), but rather allow one to calculate an $M_s = 3/2$ mixed spin state, which has contributions from $S = 7/2$, $S = 5/2$, and $S = 3/2$ states. Thus, it should be kept in mind that the $M_s = 3/2$ wave function of the {Fe−NO}^{7} systems used in

(78) Despite intensive investigation, no other peaks were observed.
(79) Nocek, J. M.; Kurtz, D. M. J.; Sage, J. T.; Xia, Y.-M.; Debrunner, P. G.; Shiemke, A. K.; Sanders-Loehr, J.; Loehr, T. M. *Biochemistry* **1988**, *27*, 1014−1024.
(80) Quinby-Hunt, M.; Feltham, R. D. *Inorg. Chem.* **1978**, *17*, 2515−2520.
(81) In the case of the NO adducts of deoxyhemerythrin, for example, no high-energy peak was ever observed, and only one low-energy peak was observed in the presence of fluoride (see ref 79).

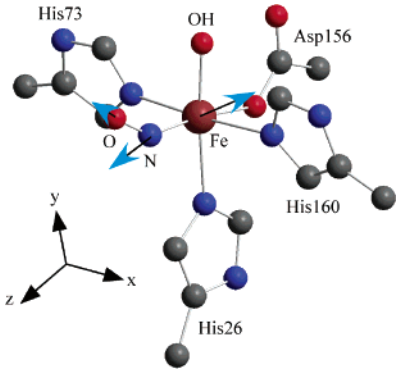

Figure 6. Active site model of NO−FeSOD based on a DFT energy minimization. The axis system is aligned according to the **D**-tensor orientation obtained from INDO/S-CI calculations. Blue arrows represent excited-state distortions relative to the ground-state equilibrium geometry associated with band 5 (Table 1) as predicted by DFT energy gradient calculations.

our computations does not describe the pure $S = 3/2$ spin state; however, this approach has been successfully employed in previous DFT studies on $\{Fe-NO\}^7$ systems.[26,36] Initial DFT energy minimizations were performed with respect to the nuclear coordinates of the nitric oxide and hydroxide ligands only. This resulted in unreasonably long Fe−N(O) bond distances (>3 Å). In contrast, full DFT energy minimization (i.e., an energy minimization with respect to all nuclear coordinates) yielded excellent agreement between optimized and experimental bond lengths reported for synthetic $\{Fe-NO\}^7$ compounds (Figure 6 and Table S1). The energy minimized species (Figure 6) exhibits an Fe−N bond length of 1.734 Å, an N−O bond length of 1.199 Å, an Fe−N−O bond angle of 145°, and an O−N−Fe−O(H) dihedral angle of 20°. For comparison, $\{Fe-NO\}^7$ systems exhibit short Fe−N bond lengths of ∼1.7 Å and N−O bond lengths of ∼1.16 Å, and the Fe−NO moiety is typically bent with an average Fe−N−O angle of 145°.[27,82] In the optimized model, the angle between the two axial histidine residues (His160 and His73) opened to 176°, an increase of 14° relative to the starting geometry based on azide-bound Fe^{3+}SOD.[4] This increase in bond angle is not unreasonable in light of the fact that azide binding to the oxidized (ferric) active site causes the N(His160)−Fe−N(His73) angle to increase from 128 to 162°,[4] revealing that this structural parameter is quite flexible and possibly indicating that the movement of these equatorial histidine residues is an important requirement for binding of substrate (analogues) to the ferrous site.[83] Overall, our model of NO−FeSOD generated by a full DFT energy minimization agrees well with similar synthetic complexes.

From pH-dependent extended X-ray absorption fine structure (EXAFS) studies on WT Fe^{3+}SOD[9] as well as combined density functional/electrostatics calculations,[11] it appears that the ferric center of Fe^{3+}SOD coordinates an axial hydroxide ligand rather than a water molecule, as present in Fe^{2+}SOD (cf. eq 1). Based on analogies with synthetic $\{Fe-NO\}^7$ systems and computational results presented below, NO binding to Fe^{2+}SOD formally oxidizes the ferrous center; thus it would seem reasonable to assume that the iron ion of NO−FeSOD also coordinates an axial hydroxide ligand. However, this assumption is challenged by the fact that significant charge is donated from the NO^- ligand to the ferric ion. To assess the protonation state of the solvent ligand in NO−FeSOD, we have employed DFT calculations to estimate the change in pK (ΔpK) that accompanies the coordination of NO to the Fe^{2+} ion. For calculating this ΔpK, we have also generated a model of NO−FeSOD, where the axial ligand is water (referred to as NO−$FeSOD^{H2O}$), and active site models of WT Fe^{2+}SOD with axial hydroxide ($Fe^{2+}SOD^{OH}$) and water ($Fe^{2+}SOD^{H2O}$) ligands. The latter two models were generated by partial DFT energy minimization, where the coordinates of all amino acid residues and the ferrous center were fixed and the coordinates of the axial solvent ligand were energy minimized. On the basis of these DFT calculations, gas-phase proton affinities ($PA_{(g)}$) were calculated for our models of NO−FeSOD and WT Fe^{2+}SOD (eq 6), and the difference in $PA_{(g)}$ between the two systems was used to estimate a shift in the pK of the axial solvent ligand associated with NO binding (eq 7). Our computations predict that the pK of coordinated water in NO−FeSOD drops by at least 3.3 pH units relative to WT Fe^{2+}SOD. During the energy minimization of NO−$FeSOD^{H2O}$, one of the two protons on the water ligand gradually moved closer to the carbonyl group of the acetate anion used to model Asp156, and in the final geometry this proton is equally shared by both the solvent ligand and the carbonyl oxygen,[84] further indicating that the ferric ion of NO−FeSOD prefers a hydroxide rather than a water ligand. As a reference value, the ΔpK for the one-electron oxidation of Fe^{2+}SOD to Fe^{3+}SOD was also calculated using a similar approach. Because our models of Fe^{2+}SOD and NO−FeSOD retain the same overall active site charge (as they merely differ by the presence or absence of a neutral NO molecule), it is reasonable to assume that changes in protein and reaction field energies (ΔE_{pr}) between these two systems are negligible. However, this assumption is no longer valid when calculating a ΔpK for the oxidation of Fe^{2+}SOD to Fe^{3+}SOD, as these two models differ in overall active site charge for a given protonation state of the solvent ligand. Therefore, we have corrected our calculated ΔpK for this oxidative process using a previously calculated ΔE_{pr} value of 32 kcal/mol.[11] On the basis of our DFT calculations and the published value for ΔE_{pr}, the one-electron oxidation of Fe^{2+}SOD is expected to increase the acidity of the axial water ligand by 32 pH units ($\Delta pK = -32$), in reasonable agreement with the computed value of $\Delta pK = -36$ by Han et al.[11] Thus, while our computational data reveal that NO binding to Fe^{2+}SOD does increase the acidity of the axial water ligand, the one-electron oxidation of the ferrous ion increases the acidity of the axial water ligand to a much greater extent, perhaps suggesting that the axial water ligand present in Fe^{2+}SOD may actually *not* deprotonate upon NO binding or that NO binding to Fe^{2+}SOD results in a mixture of NO−FeSOD species, some

(82) Feltham, R. D.; Enemark, J. H. *Top. Stereochem.* **1981**, *12*, 155−215.
(83) The larger N(His)−Fe−N(His) bond angle in the computationally derived model of NO−FeSOD relative to the crystallographically characterized active site of N_3−FeSOD probably arises from the restricted motion of the His ligands in the actual protein. However, the fact that DFT computations predict that the opening of this angle is energetically favorable when substrate analogues are bound is significant.
(84) $r(H-O^{water}) = 1.00$ Å and $r(H\cdots O^{Asp}) = 1.86$ Å for the intial structure of NO−$FeSOD^{H2O}$, whereas $r(H\cdots O^{water}) = 1.21$ Å and $r(H\cdots O^{Asp}) = 1.21$ Å in the DFT energy minimized structure. Significantly, for WT FeSOD, Asp156 hydrogen bonds with the amide backbone linking Val157 and Trp158; however, these residues are not included in our computational model. This additional hydrogen bond is expected to decrease the ability of Asp156 to develop such a strong hydrogen bond with coordinated water, and thus, it is reasonable to assume that our computations overestimate the stability of NO−$FeSOD^{H2O}$ and thereby underestimate the magnitude of the ΔpK.

Table 2. Energies (eV) and Compositions (%) of the NO π^*-Based MOs and the Fe 3d-Based MOs Based on Spin-Unrestricted DFT Computations Performed on the Active Site Model of NO−FeSOD Shown in Figure 6

orbital	cccup	spin	energy	Fe 3d	NO π^* (op)	NO π^* (ip)	OH[a]	Asp[b]	His[a]
$3d_{xy}$	1.0	↑	−6.562	54.6	0	0	20.4	1.1	10.7
$3d_{xz}$	1.0	↑	−5.963	56.6	6.2	0	0	10.9	10.2
$3d_{yz}$	1.0	↑	−5.83	41.3	0	9.37	3	25.6	0
$3d_{z^2}$	1.0	↑	−3.962	43.1	0	10.8	1.4	14.4	15.6
$3d_{x^2-y^2}$	1.0	↑	−3.439	35.2	0	20.6	19.1	4.7	9.2
NO π^* (op)	0.0	↑	−1.904	9.8	82.6	4.5	0	0	0
NO π^* (ip)	0.0	↑	−1.392	23.8	0	59.4	7.22	1.27	0
NO π^* (op)	1.0	↓	−4.283	41.4	38.7	1.4	0	7.6	0
NO π^* (ip)	1.0	↓	−3.899	26.4	0	42	8.6	14.1	0
$3d_{xy}$	0.0	↓	−2.364	76.1	0	0	16.3	0	0
$3d_{yz}$	0.0	↓	−2.079	62	1.2	26.9	0	1.4	0
$3d_{xz}$	0.0	↓	−1.704	43.1	49.5	4.4	0	0	0
$3d_{x^2-y^2}$	0.0	↓	−1.224	73.2	0	0	4.5	0	9.7
$3d_{z^2}$	0.0	↓	−0.224	30.3	0	10.4	4.3	1.3	8.8

[a] Contributions from the 2p orbitals of oxygen (for OH) and nitrogen (for His) are considered. [b] Contributions from the 2p orbitals of both oxygen atoms of the aspartate ligand are considered.

with hydroxide ligands, some with water ligands. The latter option may be ruled out, however, as it has been previously shown that EPR data collected for NO−FeSOD at pH 7 and pH 10 are virtually identical.[19] To conclusively access the protonation state of the axial ligand for NO−FeSOD, we have further evaluated the NO−FeSOD and NO−FeSOD^{H2O} models by comparing experimental data collected for NO−FeSOD with computationally predicted parameters for these two model systems.

(B) Ground-State Properties. INDO/S-CI computations were performed on both DFT geometry-optimized models of NO−FeSOD to evaluate their structures on the basis of experimental ground-state data. Unlike unrestricted DFT computations that cannot describe a pure spin state, in an INDO/S-CI treatment all spin states (i.e., the $S = 7/2$, $S = 5/2$, and $S = 3/2$ states) can be treated explicitly. An initial INDO/S computation was converged to the $S = 7/2$ state that was subsequently used as the reference state for configuration interaction (CI). As these computations were carried out to predict ground-state properties, both single and double excitations were included (CISD) within the $S = 7/2$, $S = 5/2$, and $S = 3/2$ states. For the NO−FeSOD model possessing an axial hydroxide ligand, these INDO/S-CISD computations yield an $S = 3/2$ ground state, 7100 cm^{-1} beneath the lowest energy $S = 5/2$ state. This large stabilization of the $S = 3/2$ ground state relative to the lowest $S = 5/2$ state is consistent with the temperature independence of absorption data obtained for NO−FeSOD, which indicates that the $S = 5/2$ state is not thermally populated at 300 K. These computations also properly predict the sign of D (i.e., $D = 1.6$ cm^{-1} versus the experimental value of $D > 0$ cm^{-1}) and yield a rhombicity in reasonable agreement with experimental data, i.e., $E/D = 0.179$ versus our experimental values of $E/D = 0.128$ and 0.154. Consistent with the typical electronic structure description of the {Fe−NO}^{7} moiety, the orientation of the **D**-tensor of Fe^{3+} indicates a dominant bonding interaction with NO,[32] as the principal axis of this tensor is roughly collinear with the Fe−N(O) bond. However, in the present case this axis is tilted slightly toward the hydroxide ligand (Figure 6), indicating that important bonding interactions of Fe^{3+} also exist with other ligands. This orientation of the **D**-tensor is also consistent with our analysis of VTVH MCD data collected for NO−FeSOD (Figure 4), which indicates that the prominent absorption and MCD features associated with NO^- $\pi^* \rightarrow Fe^{3+}$ LMCT transitions are polarized within the *yz* plane (vide supra). Alternatively, INDO/S-CISD computations performed on our NO−FeSOD^{H2O} model possessing an axial water ligand predict a very axial system ($E/D = 0.018$). This result agrees very poorly with our experimental data, lending further support to our hypothesis that the coordinated solvent ligand is deprotonated in NO−FeSOD.

(C) NO^-→Fe^{3+} CT Transitions. DFT computations were also used to obtain excited-state information such as electronic transition energies.[85] Electronic transition energies were determined by the method of half-electron excitation developed by Slater.[60] In this scheme, half of an electron is promoted from the donor MO to the acceptor MO, and the difference in MO energies at convergence is used as the electronic transition energy.[86] This method was previously used by Brown et al. to calculate LMCT and LF transition energies for a synthetic Fe−NO system;[26] therefore, those data will be briefly discussed so as to provide a comparison of the calculated excited-state properties of NO−FeSOD relative to those calculated for a synthetic system.

Because we were primarily interested in calculating the NO^- $\pi^* \rightarrow Fe^{3+}$ CT transition energies, the Slater method was applied to transitions involving donor and acceptor MOs that both exhibit significant NO π^* character, as these transitions are expected to carry the most absorption intensity.[87,88] The two NO π^*-based MOs can be distinguished by their orientation

(85) While INDO/S-CISD computations proved useful in the calculation of ground-state properties for our model of NO−FeSOD, this computational method preferentially stabilizes the ground state relative to excited states and thus predicts electronic transition energies that are unrealistically large. Because of this, INDO/S-CIS computations are typically used to predict electronic transition energies. For our model of NO−FeSOD, however, the $S = 3/2$ ground state calculated by the inclusion of only single electron excitations is different in composition than the $S = 3/2$ ground state calculated by the inclusion of both single and double electron excitations. Therefore, we have chosen to use DFT calculations in order to obtain excited-state properties.

(86) In this approach the calculated transition energy formally corresponds to a transition from the $M_s = 3/2$ ground state to an $M_s = 3/2$ excited state, which are not pure spin states but rather represent weighted averages of the pure $S = 7/2$, 5/2, and 3/2 ground and excited states, respectively. Thus, the calculated transition energies will be influenced by differences in the energy splittings of the ground- and excited-state spin manifolds contributing to the corresponding $M_s = 3/2$ mixed spin states. However, as these differences are expected to be small compared to LMCT energies, application of the Slater method to estimate transition energies for NO−FeSOD is reasonable.

(87) Solomon, E. I. *Comments Inorg. Chem.* **1984**, *3*, 225−320.
(88) Baldwin, M. J.; Root, D. E.; Pate, J. E.; Fujisawa, K.; Kitajima, N.; Solomon, E. I. *J. Am. Chem. Soc.* **1992**, *114*, 10421−10431.

Table 3. Relative Total Energies (kcal/mol), ZFS Splitting Parameters (cm^{-1}), and $NO^- \rightarrow Fe^{3+}$ CT Transition Energies (cm^{-1}) Based on DFT Single-Point Calculations, INDO/S-CI Calculations, and DFT Half-Electron Excitations, Respectively, Performed on Models of NO−FeSOD (with Different Fe−N−O Angles and Different O_{sol}−Fe−N−O Torsional Angles) and NO−$FeSOD^{H2O}$ [a]

	rel energy	D	*E/D*	NO $\pi_{ip}^* \rightarrow$ Fe $3d_{yz}$ (3)[b]	NO $\pi_{op}^* \rightarrow$ Fe $3d_{xz}$ (5)[b]	NO $\pi_{ip}^* \rightarrow$ Fe $3d_{z^2}$ (7)[b]
experimental		6 ± 1	0.154 and 0.128	15 500	22 700	26 900
Fe−N−O angle						
140°	1.499	1.46	0.209	15 700	20 500	26 900
145°	0	1.57	0.179	13 400	20 600	26 600
150°	1.694	1.79	0.149	14 600	20 700	26 200
O_{sol}−Fe−N−O angle						
10°	1.316	1.64	0.113	13 400	20 600	26 600
20°	0	1.57	0.179	13 400	20 600	26 600
30°	1.597	1.66	0.152	13 500	20 500	26 600
NO−$FeSOD^{H2O}$		1.54	0.018	15 500	18 600	26 700

[a] Experimental ZFS parameters and LMCT transition energies are included for reference. [b] Band numbers refer to the experimental spectra shown in Figure 3.

with respect to the Fe−N−O plane, generating an in-plane NO π^* (π_{ip}^*) MO and an out-of-plane NO π^* (π_{op}^*) MO. From Table 2, three intense $NO^- \pi^* \rightarrow Fe^{3+}$ CT transitions are expected to be observed, namely, between the NO π_{ip}^*-based spin down MO and the Fe $3d_{yz}$- and Fe $3d_{z^2}$-based spin down MOs, and from the NO π_{op}^*-based spin down MO to the Fe $3d_{xz}$-based spin down MO. The calculated transition energies obtained for the DFT geometry optimized NO−FeSOD model are in excellent agreement with our experimental data, as shown in Table 3. Significantly, these computations reproduce the large splitting ($\sim$7000 cm^{-1}) of the two lowest energy LMCT transitions, the origin of which will be discussed in detail below. By calculating similar LMCT transition energies for NO−$FeSOD^{H2O}$, it becomes clear that the presence of an axial hydroxide ligand rather than a water ligand is crucial in reproducing the experimental splitting of the $NO^- \pi^* \rightarrow Fe^{3+}$ CT transitions (Table 3). For NO−$FeSOD^{H2O}$ the splitting between the two lowest energy LMCT transitions is only 3000 cm^{-1}, a result inconsistent with experimental data. Thus, it appears that the unique ground and excited-state properties of NO−FeSOD can only be properly accounted for by considering hydroxide as the axial solvent ligand.

(D) Bonding Description. Having validated our NO−FeSOD model on the basis of structural and spectroscopic data, a detailed analysis of the calculated bonding description using both INDO/S-CISD and DFT methods is justified. In the $S = 3/2$ ground state predicted by the INDO/S-CISD method, the frontier orbitals are the five Fe 3d- and the two NO π^*-based MOs. Four of the five Fe 3d-based MOs are singly occupied, while the lowest energy Fe 3d-based MO formally carries one and a half electrons in the CI corrected ground-state wave function. This configuration describes a high-spin iron center that lies between the Fe^{3+} and Fe^{2+} formal oxidation states. However, as several of the Fe 3d-based MOs contain a significant amount of NO π^* character, the electron density present in the Fe 3d-based MOs cannot be associated solely with the Fe ion but rather is partially delocalized over the $\{Fe-NO\}^7$ system. This description offered by the INDO/S-CISD method is consistent with the DFT bonding description presented below.

DFT computations likewise reveal that the frontier orbitals of NO−FeSOD are Fe 3d- and NO π^*-based MOs (Table 2). On the basis of spin-unrestricted DFT calculated orbital compositions, the iron is best viewed as Fe^{3+}, as all Fe 3d-based spin up MOs are occupied, while their spin down counterparts are unoccupied. The NO formally carries a −1 charge, as

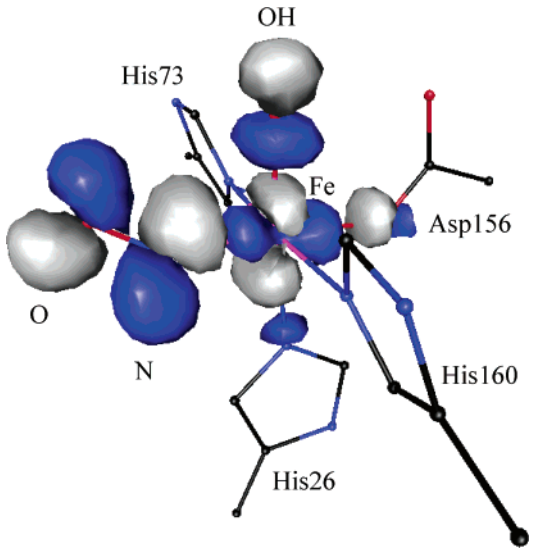

Figure 7. Boundary surface plot of the NO π_{ip}^*-based spin up LUMO.

the two spin up NO π^*-based MOs are the LUMOs, while their spin down counterparts are the HOMOs. This type of bonding has been described as Fe^{3+} ($S = 5/2$) antiferromagnetically coupled to NO^- ($S = 1$).[26,37,89] However, in the bonding description of $Fe(Me_3TACN)(NO)(N_3)_2$ given by Brown et al.,[26] the NO π_{ip}^*-based MO is at lower energy than the NO π_{op}^*-based MO, whereas our DFT computations performed on the NO−FeSOD model predict a reverse ordering. Table 2 and Figure 7 provide insight into this difference in ordering of the NO π^*-based MOs. For NO−FeSOD, the NO π_{ip}^*-based spin down MO,[90] while Fe−N(O) bonding, is σ-antibonding with respect to the Fe−OH and Fe−Asp bonds; thus, the presence of the hydroxide and Asp^- ligands destabilizes the NO π_{ip}^*-based MO to such an extent that it moves higher in energy than the NO π_{op}^*-based MO. As a consequence of this reverse ordering of the NO π^*-based MOs, the first $NO^- \pi^* \rightarrow Fe^{3+}$ CT transition is red-shifted while the second $NO^- \pi^* \rightarrow Fe^{3+}$ CT transition is blue-shifted relative to the corresponding transitions of two synthetic $\{Fe-NO\}^7$ systems,[26] resulting in a large splitting of the two lowest energy LMCT transitions (Table 3). Such perturbations relative to synthetic

(89) Li, M.; Bonnet, D.; Eckhard, B.; Neese, F.; Weyhermüller, T.; Blum, N.; Sellmann, D.; Wieghardt, K. *Inorg. Chem.* **2002**, *41*, 3444−3456.
(90) Because the NO π_{ip}^*-based spin down MO is occupied and therefore is mixed with other ligand orbitals, the bonding may be inferred from the NO π_{ip}^*-based spin down MO (Figure 7).

inorganic complexes reveal how the active site of FeSOD can influence the properties of the {Fe−NO}^{7} unit. In many Fe−NO containing model complexes, the other ligands are neutral N-donor ligands that are expected to possess a lower donor strength than the anionic hydroxide or Asp$^-$ ligands in the protein, and thus the bonding is entirely dominated by NO$^-$. As a result, the corresponding EPR spectra typically indicate an almost purely axial system. In the case of NO−FeSOD, however, the presence of strong O-donor ligands significantly affects the electronic structure of the {Fe−NO}^{7} unit. This produces a more rhombic system, as observed by EPR spectroscopy and consistent with our INDO/S-CISD computations.

(E) Excited-State Properties. The two lowest energy, spin-forbidden LF transitions for the high-spin d^5 ferric ion are the $^6A_1 \rightarrow {}^4T_1$ and $^6A_1 \rightarrow {}^4T_2$ transitions. For ferric complexes with octahedral geometry, these transitions are expected to be located at 7200−11 400 and 12 000−15 000 cm^{-1}, respectively;[91] however, the energy of these transitions will be influenced by the ligand field strength (10*Dq*) and electron−electron repulsion (the Racah *B* parameter). As the two LMCT transitions originating from the NO π_{ip}*-based MO involve excitation to Fe 3d-based orbitals deriving from the t_{2g} ($3d_{yz}$) and e_g ($3d_{z^2}$) sets, the difference in energy between these two transitions allows an estimate of 10*Dq*. This analysis reveals that for NO−FeSOD, 10*Dq* ∼ 11 400 cm^{-1}. This value compares well to literature values for octahedral ferric complexes with several anionic oxygen donor ligands, as typically 10*Dq* ∼ 10 000−14 000 cm^{-1} for such systems.[92] While for the free Fe^{3+} ion the Racah *B* parameter is B_0 ∼ 1100 cm^{-1}, the covalency of the {Fe−NO}^{7} system is expected to reduce this value appreciably. Assuming that *B* is reduced to ∼70−80% of its free ion value and using the above value of 10*Dq* ∼ 11 400 cm^{-1}, the d^5 Tanabe-Sugano diagram predicts the $^6A_1 \rightarrow {}^4T_1$ and $^6A_1 \rightarrow {}^4T_2$ LF transitions to occur within the regions of 16 500−20 500 and 20 000−24 500 cm^{-1}, respectively, for NO−FeSOD. This result is consistent with our band assignments given in Table 3 and Figure 3.

To corroborate our RR spectral analysis, distortions in the excited state corresponding to transition 5 (Figure 3, Table 1) were estimated using DFT computations by exciting a full electron from the NO π_{op}*-based spin down MO to the Fe $3d_{xz}$-derived spin down MO and calculating the energy gradients in this excited state at the ground-state equilibrium geometry. These energy gradients, which can be related to the distorting forces acting in the excited state (Figure 6), reveal that a major distortion is expected along the Fe−N(O) bond, while changes in all other coordinates should be minor. This result supports our assignment of the dominant feature at 498 cm^{-1} in the 21 834 cm^{-1} excited RR spectrum of NO−FeSOD (Figure 5) to the Fe−N stretching mode ν(FeN). Moreover, our DFT computations predict that this Fe−N bond elongation is by far the dominant distortion, providing a rationale for why other modes (e.g., the Fe−N−O bend or N−O stretch) are not observed in the RR spectra obtained upon excitation in resonance with band 5 (Table 1).

(3.3) Effect of the Second Coordination Sphere on the {Fe−NO}^{7} Unit. On the basis of kinetic studies and EPR data, it has been suggested that WT FeSOD contains a prebinding site near Tyr34 (Figure 1) that can be occupied by small anions such as chloride, perchlorate, and sulfate.[12,41] It has been assumed that this prebinding site is close to the active site of FeSOD, as the ligand binding properties of the ferric center can be affected by the partial occupation of this site. Specifically, we have previously shown that the Fe−N−N_2 angle of azide adducts of Fe^{3+}SOD (N_3−FeSOD) can be modulated by the second coordination sphere.[15] To explore whether similar second coordination sphere induced perturbations of the Fe−NO unit (e.g., due to a partial occupation of the putative prebinding site) could be responsible for the observation of two slightly different NO−FeSOD species by EPR spectroscopy, DFT and INDO/S-CI computations were performed on models of NO−FeSOD where either the Fe−N−O angle was altered from its calculated equilibrium value of 145° or the NO ligand was rotated about the Fe−N(O) bond, while all other structural parameters were left unchanged. Single-point DFT calculations performed on these modified active site models reveal that energy changes associated with an Fe−N−O angle change of 5° or a rotation about the Fe−N(O) bond by 10° are minor (note that *kT* at 298 K is ∼0.6 kcal/mol), indicating a soft potential energy surface for these distortions (Table 3).

INDO/S-CI computations were also performed on these modified NO−FeSOD models in order to explore how these structural perturbations affect ground-state properties. For all of these systems, an $S = 3/2$ ground state was predicted that lies beneath the lowest lying $S = 5/2$ state by ∼7000 cm^{-1}. Ground-state ZFS parameters, however, were affected by both the Fe−N−O angle of the model used and by rotation about the Fe−N(O) bond (Table 3). While for all Fe−N−O angles we obtained $D > 0$ cm^{-1}, the magnitude of *D* increases as the Fe−N−O angle increases, causing the system to become less rhombic. INDO/S-CI computations also reveal that rotation in either direction about the Fe−N(O) bond tends to increase *D* and thereby decrease the rhombicity. Thus, these computations reveal that minor changes in the geometry of the Fe−N−O unit cause noticeable changes in the *E*/*D* ratio, indicating that the two $S = 3/2$ signals observed in the EPR spectrum may arise from two NO−FeSOD species that possess slightly different geometries within the Fe−N−O unit.

On the basis of absorption and MCD data collected for NO−FeSOD (Figure 3), the two species observed by EPR spectroscopy (Figure 2) should have very similar LF and LMCT transition energies. Thus, DFT half-electron excitations were used to determine the effect of variations in the Fe−N−O angle or rotation about the Fe−N(O) bond on NO$^-$ $\pi^* \rightarrow$ Fe^{3+} LMCT transition energies. The results of these computations are presented in Table 3. In general, the LMCT transition energies are relatively insensitive to the Fe−N−O angle (Table 3); however, the lowest energy LMCT transition does shift to higher energy as the Fe−N−O angle is altered from its calculated equilibrium position (i.e., 145°). In contrast, rotation about the Fe−N(O) bond hardly changes the predicted transition energies of any of the three NO$^-$ $\pi^* \rightarrow$ Fe^{3+} LMCT transitions (Table 3). Thus, these computations indicate that rotation about the Fe−N(O) bond is expected to alter the LMCT transition energies less than changes in the Fe−N−O angle; however, changes in LMCT transition energies associated with either of these two structural perturbations are minor. In summary, our INDO/

(91) Neese, F.; Solomon, E. I. *J. Am. Chem. Soc.* **1998**, *120*, 12829−12848.
(92) Lever, A. B. P. *Inorganic Electronic Spectroscopy*, 2nd ed.; Elsevier: Amsterdam, New York, 1984.

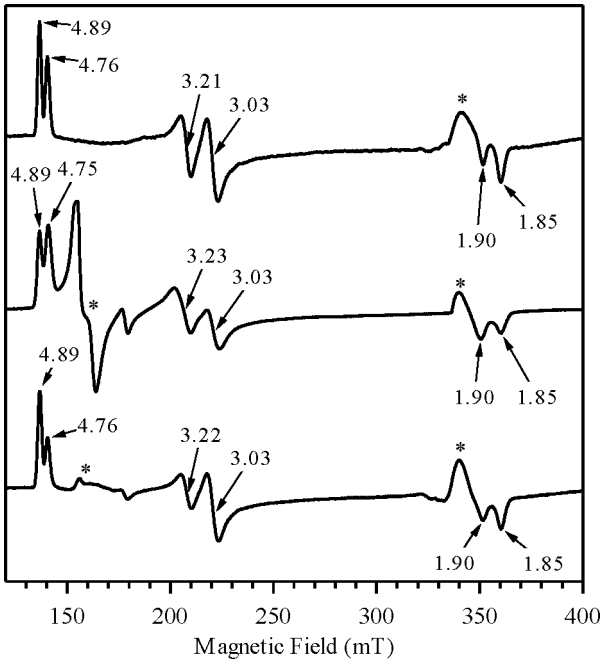

Figure 8. Top: EPR spectrum of NO−FeSOD in the presence of glycerol collected at 4 K (see Figure 2 for experimental details). Center: EPR spectrum for NO−FeSOD in the presence of 200 mM NaCl collected at 4 K, 9.3559 GHz microwave frequency, 1.27 mW microwave power, 6.3×10^4 receiver gain, 10.4 G modulation amplitude, 100 kHz modulation frequency, 5.12 ms time constant, and 2048 point resolution. Bottom: EPR spectrum for NO−FeSOD in the presence of 5 mM added $NaNO_2$ (∼7−10 mM total NO_2^- based on levels of background NO_2^-) collected at 4 K, 9.3577 GHz microwave frequency, 1.27 mW microwave power, 5.0×10^4 receiver gain, 10.4 G modulation amplitude, 100 kHz modulation frequency, 5.12 ms time constant, and 2048 point resolution. Effective g values for all EPR features associated with the $\{Fe-NO\}^7$ systems are indicated. The asterisks in the low-field region mark EPR features associated with adventitiously bound iron, while the asterisks in the high-field region mark EPR features associated with NO in frozen solution.

S-CI and DFT computations on various NO−FeSOD models reveal that small changes in the geometry of the $\{Fe-NO\}^7$ system, such as alteration of the Fe−N−O angle or rotation about the Fe−N(O) bond, are sufficient to alter the ground-state ZFS parameters of the system without markedly affecting electronic transition energies.

To experimentally explore the effect of second coordination sphere perturbations on the $\{Fe-NO\}^7$ unit, EPR data were also collected for the NO adducts of WT FeSOD (i) in the presence of 200 mM sodium chloride and (ii) in the presence of ∼10 mM sodium nitrite, as well as (iii) the NO adduct of Fe-substituted manganese SOD (Fe(Mn)SOD) from *E. coli*. In Fe(Mn)SOD, a rather strong hydrogen bond exists between Q146 (analogous to Q69 in FeSOD) and coordinated solvent,[93,94] while the first coordination sphere is essentially preserved. Comparison of the EPR spectra presented in Figure 8, top and center, reveals that at high chloride concentration the relative populations of the two $S = 3/2$ signals associated with NO−FeSOD have been altered. While at low chloride concentration (Figure 8, top) the more rhombic system ($E/D = 0.154$) has a slightly greater population than the more axial system ($E/D = 0.128$), at a higher chloride concentration (Figure 8, center), the relative populations are reversed (i.e., 58:42 at low chloride concentration versus ∼48:∼52 at high chloride concentration). Presumably, this perturbation reflects the partial occupancy of the prebinding site by chloride anion, consistent with the fact that chloride is a weak inhibitor that does not bind directly to the metal center in FeSOD.[12,41] EPR data presented in Figure 8 (cf. top and bottom) reveal that increasing the nitrite concentration can also affect the relative population of the two EPR signals; however, in this case the relative population of the more rhombic signal is enhanced (i.e., 58:42 at background nitrite concentration (∼2−5 mM) versus ∼67:∼37 at ∼10 mM total nitrite concentration). Alternatively, EPR data collected for the Fe−NO adduct of Fe(Mn)SOD (NO−Fe(Mn)SOD) reveal the presence of only one $S = 3/2$ species. Significantly, this species has g-values identical to the more axial species observed in the EPR spectrum of NO−FeSOD (cf. Figures 2 and S5). On the basis of these data, we conclude that the second coordination sphere plays a key role in determining the number and natures of the $\{Fe-NO\}^7$ systems formed when NO binds to the ferrous active site of SODs.

4. Discussion

It has been known for 15 years that Fe^{2+}SOD reacts with NO to form two $S = 3/2$ species with similar g-values;[19] however, the geometric and electronic structures of the $\{Fe-NO\}^7$ system(s) formed in this process have remained largely unexplored. Here we have used a combination of spectroscopy and computations to generate an experimentally calibrated active site model for NO−FeSOD. These data reveal that NO interacts with the five-coordinate resting site of Fe^{2+}SOD to form a six-coordinate adduct where the $\{Fe-NO\}^7$ unit is bent considerably (Fe−N−O bond angle of ∼145°), and the axial solvent ligand is hydroxide rather than water. While EPR data indicate the presence of two $S = 3/2$ species of almost equal population, electronic absorption, MCD, and RR data are consistent with the presence of only one $\{Fe-NO\}^7$ system, indicating that these two species possess similar geometric and electronic structures. INDO/S-CI and DFT computations performed on models of NO−FeSOD with different orientations of the Fe−NO unit revealed that the E/D ratio changes considerably as a function of the Fe−N−O angle or rotation about the Fe−N(O) bond, whereas $NO^- \pi^* \rightarrow Fe^{3+}$ LMCT transition energies change only slightly (Table 3), suggesting that the two species observed in the EPR spectrum of NO−FeSOD may differ only with respect to these structural parameters.

Our data indicate that several structural and electronic changes occur when NO binds to the ferrous resting state. For this five-coordinate species, access to the open coordination site is partially blocked by the two equatorial His residues (Figure 1). In light of the fact that azide binding to oxidized FeSOD was shown by X-ray crystallography to expand the N(His73)−Fe−N(His160) angle by more than 30°,[4] it is anticipated that NO binding to reduced FeSOD will also give rise to an increase in this angle. Indeed, our DFT calculations suggest that this angle opens by 48° upon NO binding, an additional 14° compared to N_3−FeSOD.[83] NO binding also has a major effect on the nature of the axial solvent ligand. While a water is bound in the reduced form of FeSOD,[9,10] DFT computations reveal that the binding of NO lowers the corresponding pK by 3.3 pH units, indicating that the acidity of coordinated solvent increases substantially upon NO coordination to the Fe^{2+} ion. Thus, it appears

(93) Vance, C. K.; Miller, A. F. *Biochemistry* **2001**, *40*, 13079−13087.
(94) Yikilmaz, E.; Xie, J.; Brunold, T. C.; Miller, A. F. *J. Am. Chem. Soc.* **2002**, *124*, 3482−3483.

reasonable to assume that a hydroxide molecule is bound as the axial ligand in the NO−FeSOD active site. Support for this proposal comes from the fact that INDO/S-CI and DFT computations performed on this active site model yield ZFS parameters and LMCT transition energies that are in excellent agreement with experimental data, whereas similar computations performed on a model of NO−FeSOD^{H2O} yield spectroscopic parameters that are incompatible with experimental data. These computational results are consistent with the results of Brown et al.[26] and Hauser et al.[37] for synthetic $\{Fe-NO\}^7$ species, indicating that nitric oxide binding to Fe^{2+}SOD is accompanied by electron transfer from the ferrous center to NO, formally generating Fe^{3+} and NO^-.

Intriguingly, while EPR data of NO−FeSOD reveal the presence of two species with similar rhombicities ($E/D = 0.154$ and 0.128), it appears that the nature and/or relative populations of these species can be altered by second sphere perturbations, e.g., by changing the nitrite or chloride concentration. The presence of nitrite in solutions of FeSOD purged with NO may imply the presence of reactive nitric oxide derivatives (e.g., nitrous anhydride, N_2O_3) that could potentially damage the FeSOD protein matrix through nitrosation of Cys or Tyr residues.[45,95,96] According to this scenario, an increase in nitrite concentration would possibly lead to higher levels of nitrosated Y34 (Figure 1), which would in turn modulate the geometry of the $\{Fe-NO\}^7$ unit, giving rise to two $S = 3/2$ EPR signals whose relative intensities would depend on the extent of nitrosation and, therefore, the nitrite concentration. The addition of chloride, which has been shown to inhibit nitrosation reactions,[45] would then simply reduce the extent to which Y34 is nitrosated and thereby alter the relative population of the two NO−FeSOD species. While this model appears consistent with some of our data, we favor an alternative explanation due to the following reasons: (i) nitrosation reactions are acid catalyzed, yet EPR data collected for NO−FeSOD at pH 7 and pH 10 by Niederhoffer et al. are virtually identical;[19] (ii) electrospray ionization-mass spectrometry studies of peptides revealed that at least 2 h of incubation with NO are required before Tyr nitrosation could be detected[95] (however, all of our samples of NO−FeSOD were incubated with NO for at most 30 min, and varying the incubation time between 5 and 30 min had no effect on the EPR spectrum); and (iii) EPR data of NO−Fe(Mn)SOD reveal the presence of only one $\{Fe-NO\}^7$ system ($E/D = 0.128$), though the active site of this system also contains a nearby Y34 residue that presumably interacts even more strongly with substrate analogues than its counterpart in FeSOD.[97] Therefore, we ascribe the presence of two $S = 3/2$ signals in the EPR spectra of NO−FeSOD to the partial occupation of the putative prebinding site (Figure 1) by anions such as nitrite or chloride, which could modulate the relative stabilities of the $\{Fe-NO\}^7$ systems formed. Kinetic experiments and EPR data suggest that a prebinding site exists in FeSOD that may be occupied by small anions, such as fluoride, chloride, and sulfate, in which case the binding properties of exogenous ligands are altered.[12,41] Alternatively, no such prebinding site has yet been observed for MnSOD.[98] Thus, the differences in NO binding between FeSOD and Fe(Mn)SOD may reflect the presence of a partially occupied prebinding site in the former protein that is absent in the latter. Studies are currently underway to explore this hypothesis and elucidate the mechanism by which the partial occupancy of the putative prebinding site is able to tune the geometric and electronic structure of NO−FeSOD.

NO−FeSOD is unique among $\{Fe-NO\}^7$ systems in that $E/D > 0.10$.[20−27] The only other known example of such a rhombic $\{Fe-NO\}^7$ system is provided by the NO adduct of protocatechuate 3,4-dioxygenase (3,4-PCD−NO) in the presence of substrate protocatechuate (PCA) and inhibitors such as homoprotocatechuate and hydroxybenzoate that are known to bind to 3,4-PCD−NO in a manner similar to PCA.[30] The active site of 3,4-PCD consists of an iron ion in a trigonal-bipyramidal geometry, coordinated axially by Tyr and His residues and coordinated equatorially by Tyr and His residues and a solvent molecule.[99] It is believed that this solvent ligand is displaced upon NO binding to form the 3,4-PCD−NO adduct.[100,101] That this $\{Fe-NO\}^7$ system gives rise to a fairly axial EPR spectrum ($E/D = 0.055$)[30] despite the fact that the 3,4-PCD−NO active site contains two anionic Tyr ligands may initially appear surprising on the basis of our results which indicate that the presence of anionic, oxygen-donor ligands tends to lead to a more rhombic system. However, spectroscopic and computational studies performed on the oxidized form of 3,4-PCD revealed that the axial Tyr ligand is oriented with respect to the ferric ion in such a manner as to create an unusually weak metal−ligand bond.[102] When PCA binds to 3,4-PCD−NO, this weakly bound axial Tyr ligand is displaced by the carbon-4 OH group of the substrate,[76] and a more rhombic EPR signal is observed. On the basis of our results for NO−FeSOD, it appears that the phenolic group of PCA interacts more strongly with the ferric ion than the axial Tyr residue. Indeed, a recent spectroscopic study of both 3,4-PCD−NO and the ternary adduct of 3,4-PCD, NO, and PCA revealed that, while the coordinating amino acid residues of both systems tend to modulate the geometric structure of the Fe−NO unit, the PCA ligand is a stronger donor ligand than the axial Tyr residue as evidenced by the blue-shifting of the $Fe^{3+} \rightarrow NO^-$ LMCT transitions.[34]

Studies of the oxidized form of FeSOD have utilized small anions such as azide to model the interaction of the ferric site with substrate superoxide, because azide and superoxide have similar frontier orbitals.[4,15] Significantly, while it has been repeatedly observed that small anions do not appear to bind to the active site of Fe^{2+}SOD,[12,17,18] our studies on NO−FeSOD reveal that NO binds to this ferrous site. Thus, the lack of anion binding to Fe^{2+}SOD does not necessarily indicate that superoxide reduction (eq 2b) occurs in an outer-sphere mechanism; rather, nitric oxide may prove to be a more suitable substrate

(95) Mirza, U. A.; Chait, B. T.; Lander, H. M. *J. Biol. Chem.* **1995**, *270*, 17185−17188.
(96) Simon, D. I.; Mullins, M. E.; Jia, L.; Gaston, B.; Singel, D. J.; Stamler, J. S. *Proc. Natl. Acad. Sci. U. S. A.* **1996**, *93*, 4736−4741.
(97) Edwards, R. A.; Whittaker, M. M.; Whittaker, J. W.; Jameson, G. B.; Baker, E. N. *J. Am. Chem. Soc.* **1998**, *120*, 9684−9685.
(98) Optical titrations of WT Mn^{3+}SOD with fluoride have previously revealed that the binding of this anion is best fit with a two-step model; thus, the first binding event may be direct fluoride coordination to the Mn^{3+} ion, while the second event may represent coordination of two fluoride molecules to the Mn^{3+} ion or binding of a fluoride molecule to a prebinding site. See: Whittaker, J. W.; Whittaker, M. M. *J. Am. Chem. Soc.* **1991**, *113*, 5528−5540.
(99) Ohlendorf, D. H.; Lipscomb, J. D.; Weber, P. C. *Nature* **1988**, *336*, 403−405.
(100) Orville, A. M.; Lipscomb, J. D.; Ohlendorf, D. H. *Biochemistry* **1997**, *36*, 10052−10066.
(101) Orville, A. M.; Lipscomb, J. D. *Biochemistry* **1997**, *36*, 6, 14044−14055.
(102) Davis, M. I.; Orville, A. M.; Neese, F.; Zaleski, J. M.; Lipscomb, J. D.; Solomon, E. I. *J. Am. Chem. Soc.* **2002**, *124*, 602−614.

analogue. While the frontier orbitals of NO and $O_2\bullet^-$ are both π^* MOs, NO is also able to mimic the open-shell nature of superoxide, as both of these species possess an $S = 1/2$ ground state where the unpaired electron density resides in these π^* MOs. In the reduction of superoxide by Fe^{2+}SOD (eq 2b), it is these π^* MOs of substrate that will accept an electron from the active site ferrous ion. Our DFT computations performed on the experimentally calibrated NO−FeSOD model reveal that when NO binds to the active site of Fe^{2+}SOD, the π^* MOs of the NO ligand acquire an additional electron. Thus, the fact that NO is able to bind to the active site of Fe^{2+}SOD and formally accepts an electron from the ferrous center suggests that the reduction of superoxide (eq 2b) could also occur by inner-sphere electron transfer.

The putative $\{Fe-O_2\}^9$ system that may be formed upon $O_2\bullet^-$ binding to the ferrous active site would differ from the $\{Fe-NO\}^7$ unit of NO−FeSOD in that the peroxide ligand is a closed-shell system with a filled set of π^* MOs and formally carries a −2 charge. Generally, $\{Fe-O_2\}^9$ systems are relatively reactive; therefore, few detailed studies of such species have been reported in the literature.[103] However, exceptions do exist,[104−107] such as the relatively stable $[Fe(EDTA)(O_2)]^{3-}$ complex that is formed upon the addition of superoxide to Fe^{2+}-EDTA or the addition of hydrogen peroxide to Fe^{3+}EDTA at high pH.[104,108,109] Spectroscopic and computational studies have revealed that this $\{Fe-O_2\}^9$ system contains a side-on η^2-peroxo Fe^{3+} core.[91,110,111] Crystallographic and spectroscopic studies on related systems have also revealed a side-on binding mode for both biological and synthetic high-spin Fe^{3+}−peroxo species.[107,112,113] However, computational studies of superoxide reductase, an enzyme that also contains a five-coordinate iron ion in the resting state,[114,115] have revealed that end-on peroxo coordination is energetically more favorable than a side-on binding mode.[116] On the basis of the structure of the FeSOD active site, it also appears unlikely that the ferric state of FeSOD could bind O_2^{2-} product in a side-on fashion similar to the $[Fe(EDTA)(O_2)]^{3-}$ complex and other related systems,[91,107,112,113] as this binding mode would require two open coordination sites. In principle, the axial water ligand (Figure 1) could dissociate upon $O_2\bullet^-$ binding, paralleling the reactivities of many dioxygenases which are known to dissociate water to accommodate other exogenous ligands.[30] However, our spectroscopic and computational data for NO−FeSOD suggest that electron transfer from the ferrous center to substrate (analogues) promotes deprotonation of coordinated water, generating a tightly coordinating hydroxide molecule. Therefore, instead of dissociating from the iron center to create an open coordination site, this axial solvent ligand releases a proton and becomes a stronger ligand. This released proton would then be optimally positioned to protonate nascent peroxide, further disfavoring the η^2 coordination geometry and promoting displacement of product. Thus, these findings support the long held assumption that coordinated solvent serves as one of the two proton donors required in the reduction of superoxide to form hydrogen peroxide (eq 2b).[2,10,12]

This and other studies reveal the importance of the axial solvent ligand and its hydrogen bond partners in tuning the reactivity of FeSOD.[15,17,93,94,117] First, this solvent ligand acts as a proton donor/acceptor, thereby facilitating release of peroxide generated in the reduction of substrate (eq 2b). Second, the formation of a tightly bound hydroxide ligand upon oxidation of Fe^{2+}SOD may prevent the product peroxide from forming a relatively stable side-on η^2-peroxo Fe^{3+} species by occupying a potential second coordination site. Third, other studies have revealed that this solvent ligand plays a critical role in tuning the reduction potential of the iron center.[93,94,117,118] The universally conserved Q69 residue develops a weak hydrogen bond to this solvent ligand when it is bound as hydroxide in the oxidized form of the enzyme and in turn destabilizes the water ligand bound to the reduced site, an effect that slightly stabilizes the oxidized form of the enzyme causing the reduction potential of FeSOD to be slightly lower than that of iron in aqueous solution. Mutation of this residue to glutamic acid (generating Q69E FeSOD) replaces the weak hydrogen bond donor with a hydrogen bond acceptor, stabilizing the reduced form of the enzyme to such an extent that Q69E FeSOD is isolated in the ferrous state and is catalytically inactive.[94] Fourth, alterations of the hydrogen bond network involving coordinated solvent tend to modulate the interaction of FeSOD with substrate analogues.[15] Indeed, our results indicate that differences in the second coordination sphere of FeSOD versus Fe(Mn)-SOD drastically affect the $\{Fe-NO\}^7$ systems formed upon addition of NO to the corresponding ferrous centers. In summary, coordinated solvent plays a crucial role in the reactivity of FeSOD; a role that is finely tuned by second sphere amino acids.

Acknowledgment. T.A.J. thanks the following: Dr. Brian Bennett (NIH/NCRR Grant RR 01008 to the National Biomedical EPR Center, MCW) of the Medical College of Wisconsin for assistance in the collection of EPR data, for simulations of EPR data, and for valuable comments on a previous version of this manuscript; Robert Clark for valuable discussions; Dr. Judith Burstyn for generously allowing use of an argon/nitric oxide apparatus; and the University of Wisconsin Biophysics Training Grant for financial support. T.C.B. thanks the University of Wisconsin and NIH (Grant GM 64631) for generous financial support and acknowledges Dr. Frank Neese (MPI Mülheim) for providing a free copy of ORCA and for useful discussions. A.-F.M. acknowledges financial support by NSF. (Grant MCB0129599).

(103) Girerd, J.-J.; Banse, F.; Simaan, A. J. *Struct. Bonding* **2000**, *97*, 143−177.
(104) Cheng, K. L.; Lott, P. F. *Anal. Chem.* **1956**, *28*, 462−465.
(105) Jensen, K. B.; McKenzie, C. J.; Nielsen, L. P.; Pedersen, J. Z.; Svendsen, H. M. *Chem. Commun.* **1999**, 1313−1314.
(106) Simaan, A. J.; Banse, F.; Mialane, P.; Boussac, A.; Un, S.; Kargar-Grisel, T.; Bouchoux, G.; Girerd, J.-J. *Eur. J. Inorg. Chem.* **1999**, 993−996.
(107) Roelfes, G.; Vrajmasu, V.; Chen, K.; Ho, R. Y. N.; Rohde, J.-U.; Zondervan, C.; la Crois, R. M.; Schudde, E. P.; Lutz, M.; Spek, A. L.; Hage, R.; Feringa, B. L.; Münck, E.; Que, L. *Inorg. Chem.* **2003**, *42*, 2639−2653.
(108) Ilan, Y.; Czapski, G. *Biochim. Biophys. Acta* **1977**, *498*, 386−394.
(109) McClune, G. J.; Fee, J. A.; McCluskey, G. A.; Groves, J. T. *J. Am. Chem. Soc.* **1977**, *99*, 5220−5222.
(110) Walling, C.; Kurz, M.; Schugar, H. F. *Inorg. Chem.* **1970**, *9*, 931−937.
(111) Ahmad, S.; McCallum, J. D.; Shiemke, A. K.; Appelman, E. H.; Loehr, T. M.; Sanders-Loehr, J. *Inorg. Chem.* **1988**, *27*, 2230−2233.
(112) Simaan, A. J.; Döpner, S.; Banse, F.; Bourcier, S.; Bouchoux, G.; Boussac, A.; Hildebrandt, P.; Girerd, J.-J. *Eur. J. Inorg. Chem.* **2000**, 1627−1633.
(113) Karlsson, A.; Parales, J. V.; Parales, R. E.; Gibson, D. T.; Eklund, H.; Ramaswamy, S. *Science* **2003**, *299*, 1039−1042.
(114) Coelho, A.; Matias, P.; Fulop, V.; Thomson, A. J.; Gonzalez, A.; Corrondo, M. *J. Biol. Inorg. Chem.* **1997**, *2*, 680−689.
(115) Yeh, A.; Hu, Y.; Jenney, F. J.; Adams, M.; Rees, D. *Biochemistry* **2000**, *39*, 2499−2508.
(116) Silaghi-Dumitrescu, R.; Silaghi-Dumitrescu, I.; Coulter, E. D.; Kurtz, D. M. J. *Inorg. Chem.* **2003**, *42*, 446−456.
(117) Vance, C. K.; Miller, A.-F. *J. Am. Chem. Soc.* **1998**, *120*, 461−467.
(118) Schwartz, A. L.; Yikilmaz, E.; Vance, C. K.; Vathyam, S.; Miller, A.-F. *J. Inorg. Biochem.* **2000**, *80*, 247−256.

Supporting Information Available: EPR data for NO−FeSOD samples prepared with 5 and 30 min of incubation time with NO (Figure S1), temperature dependence of EPR data for NO−FeSOD (Figure S2), VT MCD data (Figure S3), VTVH MCD data collected at 360, 442, and 612 nm (Figure S4), and EPR data collected for NO−Fe(Mn)SOD (Figure S5) and Cartesian coordinates for all computational models (Tables S1−S6). This material is available free of charge via the Internet at http://pubs.acs.org.

JA029523S